

THREE LINERS UNDER THE CHANDRA X-RAY MICROSCOPE

MICHAEL ERACLEOUS¹, JOSEPH C. SHIELDS², GEORGE CHARTAS¹,
 AND EDWARD C. MORAN^{3,4}
To Appear in the Astrophysical Journal

ABSTRACT

We use observations of three galaxies hosting low-ionization nuclear emission-line regions (LINERs; NGC 404, NGC 4736, and NGC 4579) with the *Chandra* X-ray Observatory to study their power sources. We find very diverse properties within this small group: NGC 404 has an X-ray-faint nucleus with a soft, thermal spectrum, NGC 4736 harbors a plethora of discrete X-ray sources in and around its nucleus, and NGC 4579 has a dominant nuclear point source embedded in a very extended, diffuse nebulosity. From their multi-wavelength properties we conclude the following about the power sources in these LINERs: the nucleus of NGC 404 is the site of a weak, compact starburst, whose X-ray emission is due to gas heated by stellar winds and supernovae, NGC 4736 appears to be in a recent or aging starburst phase, where the X-ray emission is dominated by a dense cluster of X-ray binaries, and NGC 4579 is powered by accretion onto a supermassive black hole. We detect 39 discrete sources in NGC 4736 and 21 in NGC 4579, most with $L_X > 10^{37}$ erg s⁻¹. One source in the disk of NGC 4579 appears to be an ultraluminous X-ray binary with $L_X(2 - 10 \text{ keV}) = 9 \times 10^{39}$ erg s⁻¹, but it could also be a background quasar. The most luminous discrete sources have simple power-law spectra, which along with their luminosities suggest that these are X-ray binaries accreting near or above the Eddington rate for a neutron star. By comparing the luminosity functions of discrete X-ray sources in these and other galaxies we find a potential connection between the age of the stellar population and the slope of the cumulative X-ray source luminosity function: galaxies with primarily old stellar populations have steeper luminosity functions than starburst galaxies. We suggest that this difference results from the contribution of high-mass X-ray binaries from the young stellar population to the upper end of the luminosity function.

Subject headings: galaxies: active – galaxies: nuclei – X-rays: galaxies – X-rays: binaries

1. INTRODUCTION

Low-ionization nuclear emission-line regions (LINERs; Heckman 1980) are very common in nearby galaxies; they are found in at least 30% of all galaxies and in 50% of nearby, early-type spirals. Their optical spectra feature narrow emission lines with relative strengths indicative of a low ionization state of the line-emitting gas. Although a great deal of progress has been made recently in characterizing the optical properties of LINERs (cf, Ho et al. 1997a,b,c), the nature of their power source remains controversial. This is because a number of different astrophysical processes can give rise to LINER-like optical spectra (see Filippenko 1996, for a review). The possibilities include one or a combination of the following processes.

1. The original idea suggested by Heckman (1980) was that the optical emission lines originate in shocked gas in the nucleus of the host galaxy. In their modern form, shock models can reproduce the relative strengths of many of the emission lines quite well (see Dopita & Sutherland 1995, 1996).
2. A second possibility is that the lines originate in dense gas photoionized by a hard X-ray continuum with a low ionization parameter (Ferland & Net-

zer 1983; Halpern & Steiner 1983). This hypothesis has the important implication that LINERs harbor a low-luminosity (or intermittent; Eracleous et al. 1995) active galactic nucleus (hereafter AGN). Indeed, the discovery of broad Balmer lines in the spectra of many LINERs (some of them transient or seen in polarized light) bolsters this view (Storchi-Bergmann, Baldwin, & Wilson 1993; Bower et al. 1996; Ho et al. 1997b; Barth, Filippenko, & Moran 1999; Shields et al. 2000; Ho et al. 2000; Barth et al. 2001; Eracleous & Halpern 2001).

3. Yet another possibility is that the dense gas emitting the optical lines is illuminated by a compact starburst with hot stars. This was originally considered by Terlevich & Melnick (1985), who took extreme Wolf-Rayet stars to be the dominant source of ionizing radiation. Since then this scenario has been refined and expanded to include the effects of O stars, a range of densities in the gas, and a population of post-asymptotic giant branch stars (Filippenko & Terlevich 1992; Shields 1992; Binette et al. 1994; Barth & Shields 2000).

Since LINERs are so common, improving our understanding of their power source is important and may have

¹ Department of Astronomy and Astrophysics, The Pennsylvania State University, 525 Davey Lab, University Park, PA 16802 (mce@astro.psu.edu, chartas@astro.psu.edu)

² Department of Physics and Astronomy, Ohio University, 251B Clippinger Labs, Athens OH 45701-2979, (shields@helios.phy.ohiou.edu)

³ Department of Astronomy, University of California, 601 Campbell Hall, Berkeley, CA 94720-3411, (edhead@jester.berkeley.edu)

⁴ *Chandra* Fellow

far-reaching implications. The frequency of LINERs that are weak AGNs sets a lower limit to the frequency of supermassive black holes in the centers of galaxies. If the majority are really accretion-powered sources, they would be the most common type of AGN in the present-day universe, representing the faint end of the AGN luminosity function. They could be the remnants of once ferocious quasars, and as such their demographics constrain the endpoint of quasar evolution. Moreover, the observed spectral energy distributions suggest that the accretion flows of weak AGNs in LINERs have a different structure than in Seyferts (e.g., Lasota et al. 1996; Ho 1999). They may be described by advection dominated accretion flows (ADAFs; Narayan & Yi 1994, 1995), adiabatic inflow-outflow solutions (ADIOS; Blandford & Begelman 1999), or related systems, which are interesting in their own right for understanding the growth of supermassive black holes and their radiative efficiency. In those LINERs powered by compact starbursts, the very presence of the associated young star clusters, and also their properties, constrain formation scenarios of galaxy bulges (e.g., Böker 2000). More specifically, the tidal influence of a compact star cluster in a galaxy center can destroy a pre-existing galactic bar that led to the formation of the bulge in the first place (Carollo 1999).

In view of the importance of LINERs as a class, we undertook a study of their X-ray properties with the *Chandra* X-Ray Observatory, in order to address some of the above issues. The results of previous X-ray observations have left ambiguities since older instruments had either high spatial resolution (e.g., the *Einstein* and *ROSAT* HRIs) or spectroscopic capabilities (e.g., the *Einstein* IPC, the *ROSAT* PSPC, and the *ASCA* SIS and GIS) but not both. The combination of high spatial resolution and hard X-ray response afforded by *Chandra* makes it possible to resolve such ambiguities by putting nearby LINERs under the microscope and examining their power sources in great detail. Accordingly, we have adopted the strategy of obtaining long exposures of a small number of LINERs. Our program thus complements shallower *Chandra* surveys of large, statistically complete samples of nearby galaxies, which can address different types of questions (e.g., Ho et al. 2001).

In this paper we present the results of our detailed study of 3 LINERs observed during *Chandra* Cycle 1. Included are two objects observed as part of our own guest-observer program (NGC 4736 and NGC 4579) and one object observed as part of a different program by a different group (NGC 404; the data were obtained from the *Chandra* public archive; program 01700766, P.I. P. Lira). We present the properties of the target galaxies in §2 and give the details of the observations and data reduction in §3. After describing the X-ray morphologies of the three galaxies in §4, we embark on a detailed analysis of their X-ray sources in §5–7. We conclude with a discussion of the results and their implications for the nature of LINERs as a class in §8 and §9.

2. TARGETS AND THEIR PROPERTIES

Our targets are nearby, well-studied galaxies. They are listed in Table 1 in order of increasing distance, along with their basic properties. NGC 404 is a small elliptical

galaxy while NGC 4736 and NGC 4579 are nearly face-on spirals (the latter is a barred spiral). All three galaxies were observed in the *Hubble Space Telescope* (*HST*) ultraviolet snapshot survey of nearby galaxies (Maoz et al. 1995, 1996) and were found to harbor unresolved, nuclear point sources, hinting to the presence of an AGN. Later UV spectroscopy of NGC 4579 and NGC 404 (also with the *HST*) showed the former to be a *bona fide* AGN with broad emission lines. The UV spectrum of NGC 404, on the other hand, resembles very closely that of a starburst, with prominent absorption lines from hot stars and no indication of an AGN. This result also confounds the case for an AGN in NGC 4736, since it shows that a point-like UV source could well be associated with hot stars. Narrow-band H α and [O III] images of the three galaxies, obtained from the ground and with the *HST* (Pogge 1989; Pogge et al. 2000), resolve their nuclear emission-line regions down to scales of less than 10 pc and show complex filamentary structure. It is noteworthy that the H α -emitting region of NGC 4579 is easily resolved from the ground; it extends along the direction of the bar of the host galaxy, with a projected size of approximately 3 kpc. The nucleus of NGC 4736 is surrounded by a star-forming ring of diameter 2 kpc, seen very clearly in the H α images of Pogge (1989), as well as in the radio continuum image of Turner & Ho (1994).

The target galaxies have been observed several times in the X-ray band. The two spirals are fairly bright X-ray sources in both soft and hard X-rays. Their *ASCA* spectra (Terashima et al. 1998; Roberts, Warwick, & Ohashi 1999) can be described by a composite model consisting of a hard power law with a Seyfert-like photon index of ~ 1.7 plus thermal plasma emission with a characteristic temperature in the range 0.1–1 keV, just like the spectra of most LINERs (Ptak et al. 1999). The observed luminosities are $L_X(2 - 10 \text{ keV}) = 1.5 \times 10^{41} \text{ erg s}^{-1}$ for NGC 4579 and $L_X(2 - 10 \text{ keV}) = 3 \times 10^{39} \text{ erg s}^{-1}$ for NGC 4736. Moreover, the *ROSAT* HRI image of NGC 4736 shows remarkable extended structure in the form of a halo surrounding the nucleus (Halderson et al. 2001), which is comparable in size with the star-forming ring seen in the optical emission-line and radio continuum images. The nucleus of NGC 4736 was even resolved by the *ROSAT* PSPC, which measured a soft X-ray luminosity of $L_X(0.1 - 2 \text{ keV}) = 3 \times 10^{39} \text{ erg s}^{-1}$ (Cui et al. 1997). In marked contrast, NGC 404 is extremely faint even though it is the nearest of the three targets. It was barely detected in soft X-rays by the *ROSAT* HRI with a luminosity of $L_X(0.1 - 2.4 \text{ keV}) \approx 5 \times 10^{37} \text{ erg s}^{-1}$ (Komossa et al. 1999), while an *ASCA* observation yielded only an upper limit on the hard X-ray luminosity of $L_X(2 - 10 \text{ keV}) < 5 \times 10^{37} \text{ erg s}^{-1}$ (Terashima et al. 2000a).

3. OBSERVATIONS AND DATA SCREENING

The three target galaxies were observed with the Advanced CCD Imaging Spectrometer (ACIS; Garmire et al. 2001, in preparation) on *Chandra* in 1999 December and 2000 May. The instrument was operated in faint mode. A log of observations, which includes the observation date and exposure time for each target, is given in Table 2. Their nuclei were centered on the aimpoint of the S3 CCD, which had not suffered significant radiation damage dur-

ing the early stages of the mission. In the observations of NGC 4736 and NGC 4579 only one quarter of the S3 CCD was read out; all other CCDs were turned off in order to reduce the frame time to 0.84 s, and thus to reduce the probability of photon pileup in the central pixels of bright point sources. Even with this measure, however, the bright point source in the nucleus of NGC 4579 still suffered from pileup, which complicates the spectral analysis (the circumnuclear regions of NGC 4579 were not affected). In the observation of NGC 404, 6 CCDs were turned on (4 from the ACIS-S array and 2 from the ACIS-I array), resulting in a frame time of 3.2 s. We consider here only the part of the image included on the S3 chip since this encompasses the entire optical galaxy.

The initial data screening was carried out with the CIAO software package, developed and distributed by the *Chandra* X-Ray Center (CXC). Since this software was undergoing revisions over the course of our analysis of the data, we processed the data using both versions 1.0 and 2.0 to check for consistency. Some of the later steps in the data analysis were also checked with version 2.1 of CIAO. In summary, the screening consisted of selection of events with grades 0, 2, 3, 4, and 6 and exclusion of events recorded during times of poor aspect solution and background flares. In the process we also removed the 0'.5 pixel randomization introduced during the initial data processing, which amounts to an unnecessary smearing of the image. After screening, we produced images and spectra from the photon event lists using the CIAO tools and the TARA software package (Broos et al. 2000). Below we discuss the morphology of the target galaxies as seen in the X-ray images and compare with what is seen in other bands.

4. MORPHOLOGY

Figure 2 shows a montage of the 0.5–10 keV *Chandra* images of the target galaxies. For each galaxy we present an image encompassing most of the ACIS-S3 field of view as well as a zoomed display of the nucleus. These images show exquisite detail, which we describe below in a separate paragraph for each galaxy. In our comparison with images taken at other wavelengths we have assumed that the “nucleus” of each galaxy has the same coordinates at all wavelengths. This is certainly true within the *a priori* relative astrometric uncertainties between images, which are approximately 1''.5 (dominated by the *Chandra* aspect solution; Hornschemeier et al. 2001). Because of the small field of view and bandpasses of the *Chandra* and *HST* images that we are comparing, we are not able to find matching sources that can serve to improve the relative registration of the images. We have also searched the USNO-A2.0 catalog (Monet et al. 1996) for optical counterparts to the detected X-ray sources, but found none.

- *NGC 404.* – The only significant X-ray emission within the optical extent of NGC 404 comes from a compact region associated with the nucleus. Figure 2 (top right panel) shows an image of the nucleus deconvolved via the Lucy-Richardson algorithm. There is clearly-resolved extended emission to the west and southwest of the nucleus, which after deconvolution takes the form of discrete “blobs.” The extended X-ray emission coincides with the ex-

tended UV and line emission seen in the *HST* images of NGC 404, although there is also some low-level X-ray emission as far out as 10'' from the center. Most of the flux is concentrated within 1'' from the nucleus, which corresponds to a linear scale of 12 pc. The X-ray spectrum is extremely soft, as we show in later sections. This fact along with the shell-like structure of the X-ray and emission-line images suggests that the X-ray source is hot gas, very likely associated with a superbubble blown out by a compact starburst in the nucleus of NGC 404. Contrary to the two spiral galaxies in our collection and other galaxies observed with *Chandra* (including both spirals and ellipticals; Sarazin, Irwin, & Bregman 2001; Blanton, Sarazin, & Irwin 2001; Ward et al. 2000; Mushotzky et al. 2000; Angelini, Lowenstein, & Mushotzky 2001; Lira et al. 2001; Fabbiano, Zezas, & Murray 2001) we do not find any discrete X-ray sources away from the nucleus of NGC 404, down to a limiting luminosity of 1×10^{36} erg s⁻¹. (Although there are many other sources in the field of view, none of them fall within the effective radius of the galaxy reported by Faber et al. 1989).

- *NGC 4736.* – The image of NGC 4736 shows a plethora of discrete X-ray sources, with a concentration around the nucleus of the galaxy. The collective emission from these sources, which are most likely X-ray binaries, makes up the extended, unresolved “halo” seen in the *ROSAT* HRI image, and accounts for most of the X-ray flux from this galaxy. In the innermost 400 × 400 pc of the galaxy we find a very dense cluster of 10 discrete sources embedded in a diffuse but clumpy halo. The four brightest sources (3 of which are in the central cluster) are labeled as X-1 through X-4 on the image (in order of decreasing X-ray brightness). We find that within the combined astrometric uncertainties of *Chandra* and the *HST*, the southern of the two UV point sources in the image of Maoz et al. (1995) coincides with source X-2, while the northern of the two UV sources appears to have no X-ray counterpart. The detection of large numbers of discrete X-ray sources both in NGC 4736 and in NGC 4579 (below) is undoubtedly aided by the fact that the two galaxies are oriented face-on and have a low Galactic absorption column. The spectra of the discrete X-ray sources are fairly hard and their luminosities reach values well over 10^{38} erg s⁻¹. The spectrum of the diffuse emission, on the other hand, is softer with a total luminosity comparable to that of one of the brightest discrete sources. We describe the spectral properties of the discrete sources and the diffuse emission in more detail in later sections. The large concentration of discrete X-ray sources may be associated with a recent episode of star formation, which is still ongoing to some degree in the circumnuclear star-forming ring. We discuss this possibility further in §8.2.
- *NGC 4579.* – The X-ray emission from NGC 4579 is dominated by an unresolved source coincident with the nucleus, which contributes 90% of the 2–10 keV

X-ray flux. We identify this source with the AGN, which is the source of the broad optical and UV emission lines (Barth et al. 2001; Maoz et al. 1998). The AGN is embedded in an extended, diffuse X-ray halo, which is elliptical in shape. The halo major axis is ~ 2 kpc in length, aligned approximately parallel to the bar of the host galaxy. The X-ray halo appears to coincide exactly with the $H\alpha$ emission region seen in the narrow-band image of Pogge (1989), while the much more compact $H\alpha$ -emitting region seen in the *HST* images of Pogge et al. (2000) corresponds to the innermost, brightest part of the X-ray halo, immediately surrounding the AGN. The image of NGC 4579 also shows about 20 discrete X-ray sources scattered throughout the disk of the host galaxy. These are presumably X-ray binaries, just as in NGC 4736. One of these sources, located at a projected distance of 8.7 kpc from the AGN at a position angle of 206° , is an ultraluminous X-ray binary (UXB), with $L_X(2-10 \text{ keV}) = 9 \times 10^{39} \text{ erg s}^{-1}$. It is unresolved by *Chandra*, which sets an upper limit of 120 pc to its diameter.

In the next section we present fits to the spectra of bright sources found in the three galaxies, while in later sections we study their variability and population properties.

5. MODEL FITS TO THE SPECTRA OF BRIGHT SOURCES

5.1. Extraction of Spectra

To study the spectral properties of X-ray sources in the target galaxies, we extracted their spectra using CIAO. In particular, we extracted spectra of (a) the nucleus of NGC 404 and patches of diffuse emission in the nuclei of NGC 4736 and NGC 4579, (b) the AGN in NGC 4579, and (c) the 4 brightest discrete sources (X-1 through X-4) in NGC 4736 and the extranuclear UXB (i.e. X-1) in NGC 4579. In all cases the spectra were extracted from a circular region centered on the source. The radius of this region was generally 4.1 pixels (corresponding to $2''$) for discrete sources, which encompasses more than 95% of the flux from a point source. In the case of the AGN in NGC 4579, which is quite bright and has a relatively hard spectrum, we enlarged the radius of the extraction region to 6.2 pixels (or $3''$) to include the wings of the point-spread function (PSF). In the case of the extended emission in NGC 4736, which underlies a crowded field of discrete sources, we extracted a spectrum from a region that falls SE of source X-2 and SW of source X-1. This region has a radius equal to a discrete source extraction radius and is free of discrete sources⁵. In the case of the extended emission from NGC 4579, we extracted a spectrum from an annulus centered on the AGN, with an outer radius of 20 pixels (or $9''.8$). This annulus excludes the AGN and has holes to exclude discrete sources that fall within it, as well as the “readout streak”. Its outer radius is small enough not to cross to a region of the CCD read out by a different amplifier. The response matrix and effective area curves corresponding to each source were computed automatically by CIAO after the spectrum was extracted.

A spectrum of the background for each observation was

extracted from a region of radius 50 pixels (or $24''.5$) centered in a part of the field of view that appears free of discrete sources or diffuse emission. The 0.5–10 keV background count rates in NGC 404, NGC 4736, and NGC 4579 are, respectively, 6.4×10^{-7} , 2.5×10^{-6} , and $1.3 \times 10^{-6} \text{ s}^{-1} \text{ pixel}^{-1}$, implying a total of 0.9, 6.1, and 2.3 background counts per point source, respectively (assuming a radius of $2''$). This background determination, however, applies to the particle and diffuse sky background only. The effective background for the discrete sources of interest can be considerably higher (and with a different spectrum) because these sources are embedded in diffuse emission from the host galaxy. A serious, additional complication arises from the fact that the diffuse emission is patchy and uneven, which prohibits us from using its spectrum, normalized by a geometric factor, as an effective background spectrum. To overcome this difficulty, we include the effective background in the model that we fit to discrete source spectra. More specifically, we fit the spectrum of the diffuse emission first and the model we derive for it is added to the spectral model for each source. All the parameters of the effective background model are held fixed, except for a normalization factor.

The spectra of the diffuse sources in NGC 4736 and NGC 4579 could also be contaminated by photons from the wings of the PSF of nearby, bright discrete sources. These contaminating photons have a relatively hard spectrum since the PSF is more extended at higher energies. To eliminate this contamination we simulated the images of point sources that could affect the spectra of the diffuse sources in the two galaxies using the MARX tool. From the simulated images we extracted the spectra of contaminating photons and subtracted them from the observed spectra of diffuse sources.

Spectral fits were carried out using XSPEC v.11.0.1 (Arnaud 1996). The spectra were truncated at the low end at 0.5 keV and at the high end at energies generally between 2 and 7 keV, depending on the signal-to-noise ratio (S/N). The spectral models described below were modified by interstellar photoelectric absorption with cross-sections as given by Morrison & McCammon (1983). The absorbing columns were constrained to be at least as large as the Galactic columns given in Table 1. The abundance ratios used in thermal plasma emission models are those of Anders & Grevesse (1989). The error bars given on model parameters correspond to 90% confidence intervals (for 2 interesting parameters), unless specified otherwise.

5.2. Spectra of Diffuse Sources

To model the spectrum of the diffuse emission in NGC 4736 and NGC 4579, as well as the spectrum of the nucleus of NGC 404, we tried combinations involving thermal plasma emission components (Mewe, Gronenschild, & van den Oord 1985; Mewe, Lemen, & van den Oord 1986; Kaastra 1992; Liedahl, Osterheld, & Goldstein 1995) with and without a power law. Single-temperature plasma models provide acceptable fits to the spectra of NGC 404 and NGC 4736, while a 3-temperature model is required for NGC 4579. The parameters of the best-fitting models are summarized in Table 3, and the spectra themselves are

⁵ The absence of discrete sources was verified both by visual inspection and by the systematic search described in §7

shown in Figure 3 with models superposed. The temperatures for the first two objects are around 0.6 keV, similar to what was inferred from previous *ASCA* observations of many LINERs (e.g., Ptak et al. 1999). In NGC 4579 one of the thermal emission components also has a temperature of 0.6 keV, while the other two temperatures bracket this value. It is likely that there is a range of temperatures in all cases, although this is only discernible in NGC 4579 where the *S/N* is highest. It is also noteworthy that the heavy-element abundances are considerably below their Solar values in NGC 404. In NGC 4736 and NGC 4579 the abundances are consistent with the Solar values. Keeping the abundance value in the latter object fixed to Solar yields slightly different temperatures than if the abundances were free to vary, as we indicate in Table 3.

Models consisting of thermal plasma emission plus a power-law can also yield acceptable fits, although such models are not preferable to the ones described above in a strict statistical sense. In the case of NGC 404, the power-law component has a photon index of $2.5^{+1.0}_{-0.6}$, a 0.5–2 keV luminosity of 7×10^{36} erg s $^{-1}$ and an extrapolated 2–10 keV luminosity of 5×10^{36} erg s $^{-1}$, equivalent to that of a single X-ray binary. In NGC 4579, the hottest thermal component can be substituted with a power-law component of photon index $1.5^{+0.4}_{-0.5}$ (for $Z = Z_{\odot}$). More importantly, however, the addition of a power-law to the model for NGC 404 allows us to fit the spectrum adequately by keeping the abundances fixed to their Solar values. The fundamental reason for this is that the emission-line complexes in the observed spectrum appear to be weaker than what thermal plasma models predict. Thus the addition of the featureless power law dilutes the line equivalent widths, and allows for acceptable fits with Solar metal abundances. With pure thermal plasma models, on the other hand, we can only achieve acceptable fits with metal abundances significantly less than Solar.

There are two ways of interpreting the dilution of the thermal plasma lines of NGC 404. One possibility is that the abundances are indeed lower than Solar, while the other possibility is that there is a hard X-ray source with a featureless power-law spectrum embedded in its nucleus. As we discuss in more detail in §8.1, the nucleus of NGC 404 is best interpreted as a mild starburst, which most likely hosts newly formed X-ray binaries. Therefore, we favor the latter explanation of the apparent weakness of the thermal plasma emission lines.

5.3. Spectra of Discrete Sources

We fitted the spectra of bright discrete sources with a variety of models inspired by the results of studies of X-ray binaries in the Milky Way and the Magellanic Clouds. The X-ray spectra of Galactic X-ray binaries are typically described by composite models consisting of either a multi-temperature accretion disk spectrum plus a Comptonized blackbody spectrum (motivated by *TENMA* observations; Mitsuda et al. 1984, 1989) or by a single-temperature blackbody spectrum plus unsaturated Comptonization (motivated by *EXOSAT* observations; White, Stella, & Parmar 1988). More recent observations with *BeppoSAX* and *RXTE* confirm these findings and show that these models can sometimes be indistinguishable, even with high-*S/N* spectra (see review by

Barret 2001, and references therein). The above models apply to objects in their “high” luminosity state ($L_X \sim 10^{37} - 10^{38}$ erg s $^{-1}$). As the luminosity approaches and exceeds 10^{38} erg s $^{-1}$, the spectral shape resembles a simple power law very closely. Accordingly, we experimented with combinations of soft and hard spectral components, with the soft component taken to be either a black body or a multi-color disk and the hard component taken to be a Comptonized blackbody spectrum (Titarchuk 1994) or a simple power law. We also experimented with single-component models made up of either a simple power law or a Comptonized blackbody spectrum.

We find that all spectra can be adequately described by a simple power law (resulting in $\chi^2_{\nu} \leq 1.1$), with photon indices in the range 1.1–1.8 and 2–10 keV luminosities between 4×10^{38} and 9×10^{39} erg s $^{-1}$ (the most luminous source is, of course, the UXB in NGC 4579). The parameters of the individual power-law models are given in Table 4, while the observed spectra with models superposed are shown in Figure 4. In two cases we measure absorbing columns that are almost an order of magnitude higher than the Galactic column, suggesting significant absorption in the vicinity of the source. These large columns should be regarded with caution, however, because they do not appear to be so large in all the models that we experimented with. The fact that simple power-law models provide a good description of the observed spectra is consistent with the very high luminosities of these objects, just as in Galactic X-ray binaries. Most of the other spectral models described above fit the observed spectra equally well. However, their larger number of free parameters makes them less appealing in a strict, statistical sense. Moreover, degeneracy between the model parameters and the limited *S/N* and spectral coverage prevent us from placing meaningful constraints on the parameter values. We note, nevertheless, that the fits of simple Comptonization models yield parameters comparable to those found in Galactic X-ray binaries, namely, seed blackbody temperatures between 0.2 and 1 keV, Comptonizing plasma temperatures between 2 and 5 keV, and optical depths between 2 and 6. The UXB in NGC 4579 is a notable exception in that a two-component model consisting of a multi-color disk ($kT_{\text{inner}} = 0.4 \pm 0.2$ keV) and Comptonized blackbody ($kT_{\text{bb}} = 0.5^{+0.6}_{-0.2}$ keV, $kT_{\text{compt}} < 200$ keV, $\tau < 1$) provides a somewhat better fit than a simple power-law model (χ^2 decreases by 4.71 at the expense of adding 3 more free parameters, which is significant only at the 73% level).

5.4. The spectrum of the AGN in NGC 4579

Because of its high (observed) count rate of 0.719 ± 0.005 s $^{-1}$, the spectrum of the AGN in NGC 4579 is severely distorted by the effects of pileup. In practice, the main consequence of pileup is to make the spectrum appear harder than it really is. This is a result of two effects: (a) two or more lower-energy photons arriving in the same pixel within one frame time are misidentified as single, higher-energy photons, and (b) two or more photons arriving in the same or adjacent pixels in one frame time are completely missed because they produce non-standard event grades (this affects soft photons more than hard photons because of their greater numbers). Pileup cannot yet be incorporated into the detector response matrices

and effective area curves, thus piled-up spectra must be modeled using special techniques. To this end, we have used the simulator-based, forward-fitting tool *LYNX*, developed by the ACIS instrument team (Chartas et al. 2000). This tool simulates the distribution of counts per energy channel for an assumed input spectrum and iteratively refines the parameters of the model until the simulated count distribution matches the observed one. The simulation takes into account photon trajectories (with the help of the *MARX* tool) and pileup. Uncertainties in the model parameters are computed statistically from the distribution of their values over a large number of realizations of the model. Using the above method, we were able to fit the AGN with a simple power-law model, with the absorbing column density fixed at the Galactic value. The resulting photon index is $\Gamma = 1.88 \pm 0.03$ and the 2–10 keV flux and luminosity (with pileup taken into account) are, respectively, $F_X = 5.2 \times 10^{-12}$ erg cm $^{-2}$ s $^{-1}$ and $L_X = 1.7 \times 10^{41}$ erg s $^{-1}$. This model yields a reduced χ^2 value of 0.773 for 646 degrees of freedom. The observed spectrum is shown in Figure 5 with the best-fitting model superposed for comparison. We note for reference that fitting the observed spectrum without taking pileup into account yields $\Gamma = 1.20$ and $F_X = 6.3 \times 10^{-12}$ erg cm $^{-2}$ s $^{-1}$. The degree of pileup can be quantified by the “pileup fraction”, which is defined as the ratio of the *excess* counts in a selected energy window to the true counts in that window. In this case we estimate the pileup fraction in the 0.5–10 keV band to be $f_p(0.5-10 \text{ keV}) = -0.51$ and the pileup fraction in the 6–7 keV window to be $f_p(6-7 \text{ keV}) = 0.33$. In other words, the 0.5–10 keV count rate is 1.51 times *less* than the true value and the 6–7 keV count rate is 1.33 times *more* than the true value.

To check the results of the pileup simulation, we extracted spectra of the AGN from an annulus that includes only the wings of the PSF and excludes the core where the pileup occurs. We took the outer radius of the annulus to be 6'' and we experimented with inner radii in the range 0''.5 – 1''.2. To fit these spectra we modified the effective area curves by an energy-dependent scale factor that takes into account the fact that the size of the PSF depends on energy (this factor was determined with the help of synthetic PSFs simulated with the *MARX* tool). We found that these spectra became progressively steeper as the inner radius of the annulus was increased, i.e., as more of the core of the PSF was excluded. For inner radii greater than 1'' the photon index settled to a value consistent with the *LYNX* result.

We also searched for the Fe K α line detected in previous *ASCA* observations in 1995 and 1998 by Terashima et al. (1998, 2000c), but we did not detect it. The method we adopted was to isolate the spectrum in the 4–8 keV range and fit it with a model consisting of a power-law continuum plus Gaussian emission lines at 6.4, 6.7, and 6.9 keV. The power-law model for the continuum was only a parameterization, with no particular physical significance. The effect of pileup on this portion of the spectrum is to raise the continuum level and reduce the photon index by transforming pairs of lower-energy photons into *apparent* high-energy photons. Thus, it effectively “dilutes” the observed equivalent width of any lines in this window. The amount of dilution of lines between 6 and 7 keV is the

pileup fraction estimated above, $f_p(6-7 \text{ keV}) = 0.33$. Thus all equivalent widths or upper limits determined by our procedure can be rectified by multiplying by $1 + f_p$. Accordingly, we plot in Figure 6 the 99%-confidence upper limits to the line equivalent width as a function of the assumed velocity width (FWHM). We also mark the measured equivalent widths and FWHM from the older, *ASCA* observations, which appear to be inconsistent with our upper limits. It is noteworthy that the photon index and 2–10 keV flux that we measure, also differ somewhat from what was measured by *ASCA* in 1995 ($\Gamma = 1.72 \pm 0.02$, $F_X = 4.3 \times 10^{-12}$ erg cm $^{-2}$ s $^{-1}$), but are consistent with the *ASCA* measurements from 1998 ($\Gamma = 1.81 \pm 0.06$, $F_X = 5.3 \times 10^{-12}$ erg cm $^{-2}$ s $^{-1}$). Although it is conceivable that the Fe K α line intensity has varied between the *Chandra* and *ASCA* observations, we regard this as a rather unlikely explanation since the luminosity and spectral index appear to be the same now as in the 1998 *ASCA* observation.

A more plausible and likely explanation for the difference between the *ASCA* and *Chandra* measurements is the fact that the *ASCA* spectra were extracted from a much larger region than the *Chandra* spectra and include emission from diffuse thermal plasma as well as many discrete sources. To put this difference in perspective, we note that for the AGN in NGC 4579 the area of the *ASCA* SIS extraction region ($r = 4'$) is 6,400 times larger than the area of a *Chandra* extraction region ($r = 3''$). Moreover, the radius of the *ASCA* SIS extraction region is twice as large as the radius of the entire optical galaxy. Thus any emission from hot plasma in the disk of NGC 4579 (analogous to the “Galactic Ridge” emission) is included in the *ASCA* spectrum and contributes to the strength of the Fe K α line. The fact that the line energy was 6.7 keV rather than 6.4 keV bolsters this interpretation. To make a more quantitative assessment of the plausibility of our proposed explanation, we carried out the following tests:

1. We extracted the total spectrum from the largest circular region that could reasonably fit in the *Chandra* field of view (centered on the AGN, with a radius of 50 pixels or 24''.5) and used it to look for an Fe K α line, as described above. In this spectrum we detect the Fe K α line at 68% confidence, with an equivalent width of 43 eV and we obtain an upper limit of 170 eV at 99% confidence, which is formally consistent with the *ASCA* measurement from 1998. This test illustrates that extended emission makes an increasing contribution to the equivalent width of the line in larger apertures.
2. We used the spectral models for the AGN and the diffuse emission derived from the *Chandra* observation to calculate the 2–10 keV spectrum and the *apparent* equivalent width of the Fe K α line. For the purposes of this calculation we assumed the flux and spectrum of the AGN measured above and spectrum of the extended emission determined in §5.2 and summarized in Table 3, adopting $Z = Z_\odot$ and $F_X(2-10 \text{ keV}) = 2.4 \times 10^{-13}$ erg s $^{-1}$, which is appropriate for the *entire* circumnuclear nebula. We find that the equivalent width of the Fe K α complex in the combined AGN plus circumnuclear plasma

spectrum is approximately 40 eV. This implies that the entire strength of this line complex measured by *ASCA* can be accounted for, if we allow the entire galaxy to have 6 times the emission measure of the circumnuclear region, which is a reasonable possibility.

6. VARIABILITY OF BRIGHT SOURCES

To study the variability properties of the bright discrete sources in NGC 4736 and NGC 4579, we extracted their 0.5–8.0 keV light curves from the same spatial regions used to extract spectra. Since only one quarter of the S3 CCD was read out during the observations of these two galaxies, the frame time was 0.84 s. In the case of the AGN in NGC 4579 pileup is a cause for concern since it affects the properties of the light curve. The qualitative effect of pileup is to dilute the amplitude of any variability since it leads to some pairs of lower-energy photons being counted as single, higher-energy photons. Moreover, pileup also decreases the S/N since some photon grades are transformed to unacceptable grades and those photons are not counted at all. The magnitude of these effects cannot be quantified without detailed and extensive simulations, which are well beyond the scope of this work. We have nevertheless made an effort to minimize the effects of pileup on the light curve of the AGN by restricting the band to 0.5–1.0 keV. This narrow, soft band encompasses the peak of the instrument sensitivity, thus including a significant fraction of the detected photons. The fact that it spans only a factor of 2 in energy means that any pairs of lower-energy photons that are counted as one will not be included in the band. Contamination by pairs of photons below 0.5 keV counted within this band is small because the sensitivity of the CCD declines steeply below this energy. Hence, the most significant effect of pileup on light curves from this band is to reduce the S/N somewhat. Yet another way of minimizing the effects of pileup on a light curve is to extract the light curve after excluding the core of the PSF, where pileup really occurs (cf, §5.4). Thus we have also extracted a light curve from an annulus with inner and outer radii of $0''.5$ and $4''.2$ respectively, which includes approximately half of the total counts.

In Figure 7 we show the light curves of all the bright discrete sources in the two galaxies, binned into 30-minute time bins. These light curves show that the discrete sources vary on time scales of a few hours at the 20–30% level, while the AGN varies at the 5–10% level. The magnitude of the variability is quantified by applying the excess variance test (Nandra et al. 1997a) to these light curves, whose results are summarized in Table 5. In the case of NGC 4579, the excess variance computed from the soft light curve agrees with the value obtained from the outer-PSF light curve and is a factor of 2 higher than the full-band light curve. This suggests that pileup dilutes the variability in the full-band light curve but not in the other two light curves. It also suggests that the shape of the spectrum does not change as the light curve flickers. The level of variability of the AGN in NGC 4579 is higher than what is observed in typical LINERs of comparable luminosity (Ptak et al. 1998) and approaches that of Seyfert galaxies whose luminosities are 1–2 orders of magnitude higher than that of NGC 4579. Unfortunately,

it is difficult to draw more extensive conclusions from the variability properties of the nucleus of NGC 4579 because of the caveats associated with pileup.

We have also searched for coherent, periodic signals in the light curves of the bright discrete sources, but no such signals were found. We carried out this search by computing the Fourier transforms of the source light curves up to frequencies of 0.6 Hz, following the methodology of Eracleous, Patterson, & Halpern (1991). Using the noise properties of the power spectra we have estimated upper limits to the amplitudes of undetected signals, which we list in Table 5. These limits are expressed as a minimum detectable “pulsed fraction,” which is the amplitude of a sinusoidal signal relative to the mean level of the light curve.

7. DETECTION AND POPULATION PROPERTIES OF THE DISCRETE X-RAY SOURCES

To study the population of discrete X-ray sources in the target galaxies, we used the source detection program **WAVDETECT** (Freeman et al. 2001), which is included in the **CIAO** package. We searched for sources on several spatial scales (from 1.4 to 11.6 pixels, in steps of $\sqrt{2}$), accepting detections associated with less than 10^{-6} chance probabilities due to local background fluctuations. We repeated the search twice, first in the full, 0.5–8 keV, band and then in the soft, 0.5–2 keV, band. We combined the results of the two passes to compute an X-ray color for each source, which we define as the ratio of counts in the hard (2–8 keV) band to counts in the soft (0.5–2 keV) band. Because the sensitivity of the instrument rises steeply towards low energies, all of the sources are detected in the total and soft bands, but nearly half of the sources have a hard band count rate consistent with zero. In the end our detection limit corresponds to about 6 counts per source, although it varies over the field of view because of (a) vignetting, (b) degradation of the image quality off axis, and (c) patchy diffuse emission, which increases the effective local background. After carrying out the above automatic procedure, we checked the measured properties of many of the detected sources manually. We paid particular attention to sources in the crowded field in the nucleus of NGC 4736 and we excluded any sources falling along the readout streak in the image NGC 4579. We tabulate the properties of detected sources in Tables 6 and 7, where we give the coordinates of each source, the total count rate, the X-ray color, and an estimate of the 0.5–8 keV luminosity. For sources whose hard count rate is consistent with zero, we only give an upper limit to the color.

To estimate the luminosities given in the source tables we assumed that the source spectra could be described by a simple power law with an absorbing column equal to the Galactic column. With this assumption we simulated spectra with a wide range of photon indices (0.5–5.0) and measured and tabulated their colors and count rates in the same way as we did for the observed spectra. We used the resulting lookup table to estimate the photon indices and fluxes of detected sources from their observed colors and count rates. By comparing the results of this method with results obtained for bright sources for which spectra were extracted and fitted with models, we estimate the uncertainty in the photon index and flux to be about 10–20%.

This uncertainty is in addition to the Poisson uncertainty on the count rate listed in Tables 6 and 7. In cases when only an upper limit to the color was determined from the data, we used this upper limit to determine the photon index. Thus the uncertainty in the flux of these sources can be up to 50%, judging from the relation between photon indices and count rates in simulated spectra.

As we already mentioned in §4, in NGC 404 we do not find any X-ray sources other than the nucleus, down to a limiting luminosity of 1×10^{36} erg s $^{-1}$. In NGC 4736 and NGC 4579 we find respectively 39 and 21 sources, with luminosities in the range $1 \times 10^{36} - 1 \times 10^{39}$ erg s $^{-1}$ in the former galaxy and $1 \times 10^{37} - 9 \times 10^{39}$ erg s $^{-1}$ in the latter. The lower end of the range is effectively our detection limit. Thus, in the case of NGC 4736 we can detect typical supernova remnants (SNRs) and Be-star X-ray binaries (BeXBs), while in the case of NGC 4579, we can detect low-mass X-ray binaries (LMXBs) or more luminous objects. We have estimated the probability of contamination of the source population by unrelated, background sources using the number counts of sources derived from deep *Chandra* surveys by Tozzi et al (2001). In the observation of NGC 4736 the limiting flux is 4.8×10^{-16} erg cm $^{-2}$ s $^{-1}$, which yields an expectation value of 5 background sources within the field of view, while in the observation of NGC 4579 the limiting flux is 5.6×10^{-16} erg cm $^{-2}$ s $^{-1}$ and the expected background source number is 4. These are conservative upper limits to the number of background sources, since the flux of such sources would be attenuated as it passes through the disk of the foreground galaxy. If we assume, for example, that the column density perpendicular to the galactic disks is 1×10^{21} cm $^{-2}$, the expected number of background sources in each case decreases by 1. Thus, contamination from background sources is negligible from the point of view of our statistical studies, although it may be an issue in our discussion of the properties of individual sources. We also considered the possibility of foreground contamination, i.e. that some of the detected X-ray sources are foreground stars. The absence of optical counterparts of any of the detected X-ray sources (see §4) indicates that there is no foreground contamination. This is not unexpected since the Galactic latitude of the target galaxies is rather high (-27° , $+76^\circ$, and $+74^\circ$ for NGC 404, NGC 4736, and NGC 4579 respectively). The faintest optical objects that could be associated with detected X-ray sources are M stars. Using the X-ray-to-optical flux ratios of M stars reported by Hempelmann et al. (1995), we estimate that M star counterparts to the sources that we have detected should have $R < 20.2$, and would have been included in the USNO A2.0 catalog.

The spatial distribution of sources differs markedly between NGC 4736 and NGC 4579. In the former galaxy there is a concentration of sources within $10''$ from the nucleus, and a separate concentration at the radius of the star-forming ring (~ 45 – $50''$). Thus, the distribution of X-ray sources does not follow the distribution of infrared light (i.e., starlight) from the host galaxy, but rather the distribution of emission-line light (cf, Smith et al. 1994), suggesting a connection with star formation. In contrast, the sources in NGC 4579 are distributed smoothly with distance from the center.

In Figure 8 we show the “color-magnitude” diagrams

and the luminosity distributions of the source populations of the two galaxies. In both galaxies, the most luminous sources have photon indices between 1.0 and 2.0. At lower luminosities only limits on the photon index are available, although there are some notable exceptions in both galaxies, where we detect rather hard sources ($\Gamma \sim 1$) at $L_X \sim 10^{37}$ erg s $^{-1}$. The luminosity distribution appears to peak just below 10^{37} erg s $^{-1}$ in NGC 4736 and just below 10^{38} erg s $^{-1}$ in NGC 4579.

In Figure 9 we compare the cumulative X-ray source luminosity functions of NGC 4736 and NGC 4579 with those of other galaxies with published *Chandra* data. We include two early-type galaxies, NGC 4697 and NGC 1553 (E and S0, respectively; Sarazin et al. 2001; Blanton et al. 2001) and two starbursting spirals, M82 and the Circinus galaxy (Griffiths et al. 2000; Bauer et al. 2001). NGC 4579, NGC 4697, and NGC 1553 stand out in this figure because their cumulative X-ray source luminosity functions are steeper than those of the other three galaxies. This difference can be quantified by fitting a simple power-law model [$N(L) \propto L^{-\alpha}$ or $N(> L) \propto L^{-(\alpha-1)}$] to the data at luminosities above the initial plateau. In the case of NGC 4579, NGC 4697, and NGC 1553 we find power-law indices (α) between 2.0 and 2.4, while in the other two galaxies the power-law indices range between 1.4 and 1.6. In fact, the difference is more extreme than what the above power-law indices indicate because the X-ray luminosity functions of the two early-type galaxies steepen at luminosities higher than about 10^{38} erg s $^{-1}$ (Sarazin et al. 2001; Blanton et al. 2001).

It is interesting to note that the galaxies with steep X-ray source luminosity functions are the ones without signs of current or recent star formation activity. In this context it is noteworthy that a similar effect is observed in two nearby spiral galaxies, M31 and M81 (Primini, Forman, & Jones 1993; Tennant et al. 2001), where the X-ray luminosity functions of bulge and disk sources have been measured separately. The bulge luminosity functions resemble those of early type galaxies, while the luminosity function of the disk of M81 resembles that of the starbursting spirals (the disk luminosity function of M31 has not been reported). In §8 we interpret this difference in X-ray source luminosity functions by appealing to current or recent intense star formation and the age of the underlying stellar population.

8. DISCUSSION

8.1. Implications for the Central Engines of LINERs

Our original aim in undertaking this program was to search for the power source of the optical emission lines, which are the hallmark of LINERs. Our main result is that the objects in our small collection are quite diverse in their properties, with a different power source apparently playing the dominant role in each galaxy. As a first step in considering the implications of these findings, we compare them with published results of previous X-ray observations of these galaxies with *ASCA*. In Table 8 we list the 0.5–10 keV luminosity of the different components contributing to the X-ray emission from each galaxy. This table quantifies the general description given in §4. The sum of these components reproduces fairly closely the flux detected by *ASCA* from each of these galaxies. One notable discrepancy between the *Chandra* and *ASCA* spectra

is the detection of Fe $K\alpha$ lines at 6.4 and 6.7 keV in the *ASCA* spectra of both NGC 4736 and NGC 4579 (Roberts et al. 1999; Terashima et al. 1998). Such lines are not seen in the *Chandra* spectra of any of the bright discrete sources in these galaxies. What *Chandra* does detect, however, is a hot component ($kT \sim$ several keV) to the plasma that permeates the central regions of these two galaxies. The discrepancy can thus be resolved if the Fe $K\alpha$ emission lines in the *ASCA* spectra arise from this hot plasma, as discussed in §5.4.

In NGC 4579 the case for an AGN seems iron clad. A central, compact source dominates the power budget, as we illustrate in Table 8. The spectral energy distribution of this source has a significant contribution from UV light, broad optical and UV emission lines, as well as a non-thermal radio spectrum with a brightness temperature of 2×10^8 K (Falcke et al. 2000). All these properties are classic traits of an AGN.

At the opposite extreme, NGC 404 harbors a rather anemic star-forming region in its nucleus. Its X-ray luminosity of 1×10^{37} erg s $^{-1}$ is comparable to that of a single HMXB or a giant star-forming region such as 30 Doradus (cf, Wang & Helfand 1991). The soft, thermal X-ray spectrum favors an origin of the X-rays in the hot gas of a superbubble, powered primarily by off-center supernovae (see the discussion by Chu & Mac Low 1990). This view is supported by the absorption-line UV spectrum and the monochromatic luminosity at 2270 Å of $L_\lambda(2270 \text{ Å}) = 1.2 \times 10^{36}$ erg s $^{-1}$ Å $^{-1}$ (from Maoz et al. 1995), which is equivalent to that of 10 late-O supergiants. The sound speed in the hot gas is of order $c_s \approx 380 (kT/0.5 \text{ keV})^{1/2}$ km s $^{-1}$, which is considerably larger than the velocity dispersion of the stars in the nucleus of the galaxy ($\sigma_* = 55$ km s $^{-1}$; Faber et al. 1989). Thus the gas must be unbound, a conclusion bolstered by the “blow-out” morphology of the H α + [N II] image, which also lends support to the superbubble hypothesis for the X-ray emitting gas.

In the case of NGC 4736, there is no compelling evidence for the presence of an AGN even though this galaxy is fairly bright in X-rays and harbors an unresolved UV source. The X-rays are produced by a dense cluster of stellar X-ray sources in the inner 2 kpc of the galaxy, and to a lesser degree by diffuse emission from hot gas (see the energy budget in Table 8). This possibility was correctly anticipated and discussed by Roberts et al. (1999) and Roberts et al. (2001) who nonetheless preferred an AGN interpretation in the end. As we argue below, these X-ray sources could have been produced in a recent episode of star formation and probably consist of high-mass X-ray binaries (HMXBs), LMXBs, and SNRs. The brightest nuclear X-ray sources have very similar X-ray spectra and comparable luminosities, making the association of any one of them with an AGN rather implausible. It should be pointed out, however, that source X-2, coincides with the nuclear UV source detected by the *HST*; thus it stands out among the nuclear X-ray sources as the only one with a UV counterpart. But even if we associate this source with an AGN, it is not very important energetically since it contributes less than 20% of the

X-ray luminosity and less than half of the UV luminosity.⁶ The properties of the non-thermal radio continuum emission from the nucleus (Turner & Ho 1994) are consistent with an origin in a group of several, young SNRs of the Cas A variety, whose kinetic energy heats the gas responsible for the diffuse X-ray emission (cf, the discussion of the diffuse X-ray emission of the LMC by Wang et al. 1991). In the same spirit, the nuclear, point-like, UV source is very likely an OB association, which hosts a HMXB (NGC 4736 X-2). The observations of Maoz et al. (1995) provide a lower limit to the monochromatic luminosity at 2270 Å (the central point source is saturated) of $L_\lambda(2270 \text{ Å}) > 4.4 \times 10^{36}$ erg s $^{-1}$ Å $^{-1}$, which is equivalent to the luminosities of 5 late-O supergiants. Independent evidence from optical spectroscopy by Taniguchi et al. (1996) leads to similar conclusions about the nature of the activity in the nucleus of NGC 4736. These authors find that the optical absorption-line spectrum of the nucleus of NGC 4736 agrees with models of a 10^9 -year old starburst. They also find that the nuclear H α luminosity is no larger than that of luminous Galactic H II regions and that six O6 stars are enough to power it. Thus, this particular LINER seems to be associated with a recent or aging starburst rather than an AGN.

8.2. The Discrete Source Populations

The discrete sources detected in NGC 4736 and NGC 4579 may include a variety of objects. The most luminous sources ($L_X > 10^{37}$ erg s $^{-1}$) are most likely X-ray binaries: a combination of LMXBs and HMXBs. This conclusion is supported by two pieces of evidence: their spectra, which are similar to those of bright Galactic X-ray binaries, and their variability properties, which suggest that these are individual objects, rather than clusters of less luminous sources. Other types of object, such as SNRs and BeXBs, could contribute to the population of lower luminosity sources, detected primarily in NGC 4736. If we could determine the colors of the lower-luminosity sources we could perhaps use them to differentiate between SNRs and BeXBs since the 2–10 keV spectra of the former are dominated by line emission at low energies, while the spectra of the latter resemble power laws.

The high concentration of luminous sources in the nucleus of NGC 4736 suggests that we are observing the aftermath of an intense episode of star formation. By extension, a significant fraction of the discrete sources in NGC 4736 could be HMXBs rather than LMXBs. Models of populations of interacting binaries associated with bursts of star formation (Cerviño, Mas-Hesse, & Kunth 1997; Van Bever & Vanbeveren 2000; Sipior & Eracleous 2000) show an initial hard-X-ray luminous phase, which is intimately connected with the rise and fall of HMXBs (see also the discussion of the processes by Dalton & Sarazin 1995). The first HMXBs make their appearance after the death of the most massive O stars, and shine brightly until the demise of their O and B secondaries. At this point the total hard X-ray luminosity of the population should decline until the first luminous LMXBs arrive on the scene, causing the X-ray luminosity to level off with time. Thus, the hard X-ray emission from the population should per-

⁶ For the sake of completeness, we note that the stellar velocity dispersion of NGC 4736 of 136 km s $^{-1}$ (Mc Elroy 1995) implies a black hole mass of $2 - 3 \times 10^7 M_\odot$ and an Eddington ratio of $L/L_{\text{Edd}} \approx 3 \times 10^{-6}$ (see §8.4 for the details of the methodology).

sist for up to 50 Myr after the vigorous star formation has stopped. Inspired by the model predictions, we propose that the nucleus of NGC 4736 is an “aging” starburst or in an immediate post-starburst phase, where the HMXBs dominate the top of the X-ray source luminosity function. In support of our hypothesis we note the qualitative difference between the cumulative luminosity functions of X-ray sources in nearby galaxies, shown in Figure 9 and discussed in §7. Galaxies currently undergoing vigorous star formation, such as M82 and Circinus, have cumulative luminosity functions that are flatter than those of galaxies with primarily old stellar populations such as NGC 4697 and NGC 1553. We speculate that the flatter slopes result from an excess of luminous HMXBs that have formed recently. The steep luminosity function of NGC 4579 fits well within this picture since there are no indications of ongoing, intensive star formation in its bulge or disk.

A particularly striking source is NGC 4579 X-1, which could be a UXB. If this object is at the distance of NGC 4579, as we have been implicitly assuming, its 2–10 keV luminosity would exceed 10^{40} erg s $^{-1}$. Its spectrum is very similar to the spectra of the X-ray binaries in NGC 4736 and, in fact, it is the only one of the bright X-ray sources whose spectrum is better described by a Comptonized blackbody model than by a simple power law. This object is consequently very similar to luminous Galactic X-ray binaries. Its luminosity corresponds to the Eddington limit for a 70 M_{\odot} object, which could be regarded as a lower limit on the mass of the accreting compact object, at first glance. However, the Eddington limit need not apply in the non-spherical accretion geometry of X-ray binaries, and a number of cases are known in which it is blatantly violated. There are at least 3 X-ray pulsars in the Magellanic Clouds (LMC X-4, SMC X-1, and A 0538–66; Nagase 1989; Woo, Clark, & Levine 1995, and references therein) whose luminosities exceed the Eddington limit for a neutron star by as much as a factor of 5 (and even by a factor of 30 in the flares of LMC X-4; Woo et al. 1995). Of course violations of the Eddington limit may be transient (cf. the discussion of SMC X-1 by Helfand & Moran 2001) or merely appear as such because of beaming (King et al. 2001). However, the fact remains that at certain times or from certain viewing directions some X-ray binaries appear extremely luminous. Thus, the accreting compact object in NGC 4579 X-1 need not be more massive than about 10 M_{\odot} . Another possibility is that this source is at a large distance behind NGC 4579. The fact that we expect 3 background sources in the image of NGC 4579, as well as the large measured column density (comparable to the column density perpendicular to the disk of a spiral galaxy) make this a plausible scenario. It should be pointed out, however, that the 3 expected background sources should be rather faint according to the flux distributions measured in deep surveys. The *a priori* probability of finding a background object with the 2–10 keV flux of NGC 4579 X-1 in our field of view is approximately 6%. If this source were a background AGN, then its redshift, as inferred from the observed flux, would be $z = 0.01$ ($H_0/50$ km s $^{-1}$ Mpc $^{-1}$) ($L_X/10^{42}$ erg s $^{-1}$) $^{1/2}$, suggesting that the source could easily be a garden variety Seyfert galaxy at $z = 0.01$ or a luminous quasar at $z = 1$. Ascertaining the nature of this source will have to await

identification of its optical counterpart.

8.3. The AGN and Extended Emission in NGC 4579

Using the uncontaminated luminosity of the AGN in NGC 4579, we can explore the properties of the accretion flow onto the supermassive black hole that powers it. We can estimate the mass of the central black hole using recently established correlations between it and the velocity dispersion of stars in its immediate vicinity (Gebhardt et al. 2000; Merrit & Ferrarese 2001). The velocity dispersion of 185 km s $^{-1}$ measured by Dressler (1987) yields a black hole mass in the range 6 to $13 \times 10^7 M_{\odot}$, comparable to what is found in Seyfert galaxies (Ferrarese et al. 2001). Assuming that the observed 0.5–10 keV luminosity is about 10% of the bolometric luminosity, we can estimate the Eddington ratio for this AGN to be $L/L_{\text{Edd}} \approx 1 - 2 \times 10^{-4}$, which is a low value, consistent with expectations for a low-luminosity AGN. At such a low Eddington ratio, the inner accretion flow is expected to be advection-dominated (an ADAF or similar structure) and thus very hot, vertically extended, and optically thin. Such a structure would be very different from a conventional, optically thick, geometrically thin accretion disk in its observational signature. In particular, the absence of an optically thick inner accretion disk can explain the weakness of the Fe K α line of NGC 4579 relative to what is observed in Seyfert galaxies (see the detailed discussion in Eracleous, Sambruna, & Mushotzky 2000). A vertically extended ADAF comprising the inner accretion structure can illuminate the outer thin disk and drive the emission of optical Balmer lines as well as X-ray Fe K α lines. This scenario offers an appealing explanation for the double-shouldered profile of the H α line of NGC 4579 (Barth et al. 2001) just as it does for the double-peaked Balmer lines in broad-line radio galaxies (Eracleous & Halpern 1994). However, models for the continuum spectra of ADAFs (e.g., Narayan, Yi, & Mahadevan 1996) predict X-ray spectral indices flatter than the typical values observed in Seyfert galaxies. This does not seem to hold for NGC 4579, where the 2–10 keV spectral index is typical of a Seyfert galaxy but the equivalent width of the Fe K α line is not. However, the UV-X-ray spectral index (α_{ox}) of NGC 4579 is rather typical of LINERs as shown by Ho (1999). Interestingly enough, the variability amplitude is also high for a low-luminosity AGN and is comparable to what is observed in Seyferts (see §6). Therefore, NGC 4579 appears to be a “hybrid” object with some properties characteristic of Seyferts and other characteristic of LINERs or low-luminosity AGNs.

The heating mechanism of the extended emission region of NGC 4579 is unclear. We can confidently exclude any mechanical interaction between it and an AGN jet since the VLBI radio images of Falcke et al. (2000) show only an unresolved radio core with no extension. One possible mechanism is that the extended emission region is photoionized by the AGN. The X-ray luminosity of the AGN is 20 times higher than that of the circumnuclear nebula and a fraction of the hard X-ray luminosity from the circumnuclear region may be contributed by BeXBs and LMXBs, which we have not detected. Thus, photoionization may be a viable mechanism. Moreover, as Maoz et al. (1995) point out, the extrapolation of the observed UV

luminosity is enough to power the optical emission lines from the same region. Another mechanism is heating by stellar processes in the wake of a circumnuclear starburst. In the context of this scenario, the starburst should be old enough that its luminous O stars have passed away and supernova remnants have blended together into a diffuse circumnuclear medium. Unfortunately, we cannot assess the likelihood of the above scenarios with the information currently available.

9. EPILOGUE

The results of our exploratory observations indicate that LINERs are a heterogeneous population of objects. This should not come as a surprise, in view of the way that the class is defined. But an important question that remains outstanding is what fraction of LINERs are powered by accretion onto a supermassive black hole and how these objects can be identified unambiguously. Unfortunately, the first part of this question cannot be answered until the second part is answered first. One rather clear signature of an AGN is the presence of broad emission lines in the optical or UV spectra of LINERs. However, the absence of broad emission lines cannot be taken as evidence that there is no AGN. This is especially true when one considers the practical difficulties of finding weak broad lines in the starlight-dominated spectra of LINERs. Another possibly clear signature of an AGN is the presence of a non-thermal radio core with a high brightness temperature.

X-ray observations can also shed light on this question, although they are more demanding in terms of resources and may not always yield a definitive answer. The high

spatial resolution of *Chandra* now allows us to examine the morphology of LINER nuclei in detail and combine morphological and spectral information, just as we have done here. However, one can also envisage cases where a LINER harbors a single, discrete source of “intermediate” luminosity (10^{39} – 10^{40} erg s $^{-1}$), which could equally well be an AGN or a UXB. Moreover, observations with *ASCA* should be regarded with caution, since they can sometimes be misleading because of their poor spatial resolution. A good case in point is provided by NGC 4736, whose X-ray binaries and diffuse emission produce a spatially integrated spectrum that can be modeled by a hard power law and a thermal plasma component. This “canonical” LINER spectrum can result from a current or recent starburst, just as well as it can result from an AGN.

This work was supported by NASA through grant GO0-1152A,B from the Smithsonian Astrophysical Observatory. E.C.M. is supported by NASA through *Chandra* Fellowship grant PF-10004, awarded by the *Chandra* X-ray Center, which is operated by the Smithsonian Astrophysical Observatory for NASA under contract NAS8-29073. We are grateful to Ann Hornschemeier for many helpful discussions and technical advice. We thank Lars Bildsten, Bob Rutledge, and Dani Maoz for useful suggestions. We also owe thanks to Rick Pogge and Dani Maoz for providing us with optical images of our target galaxies in a convenient, electronic format, and to Franz Bauer for doing the same with the luminosity functions of X-ray sources in nearby galaxies.

REFERENCES

- Anders, E. & Grevesse, N. 1989, *Geochimica et Cosmochimica Acta*, 53, 197
- Angelini, L., Loewenstein, M., & Mushotzky, R. F. 2001, *ApJ*, 557, L35
- Arnaud, K. 1996, in *ASP Conf. Ser. 101, Astronomical Data Analysis Software and Systems V*, eds. G. Jacoby & J. Barnes (San Francisco: ASP), 17
- Barret, D. 2001, in “Proceedings of 33rd COSPAR Scientific Assembly (Warsaw, July 2000),” *Advances in Space Research*, in press (astro-ph/0101295)
- Barth, A. J. & Shields, J. C. 2000, *PASP*, 112, 753
- Barth, A. J., Filippenko, A. V., & Moran, E. C. 1999, *ApJ*, 525, 673
- Barth, A. J., Ho, L. C., Filippenko, A. V., Rix, H.-W., & Sargent, W. L. W. 2001, *ApJ*, 546, 205
- Bauer, F. E., Brandt, W. N., Sambruna, R. M., Chartas, G., Garmire, G. P., Kaspi, S., & Netzer, H. 2001, *AJ*, in press (astro-ph/0104035)
- Binette, L., Magris, C. G., Stasinska, G., & Bruzual, A. G. 1994, *A&A*, 292, 13
- Blandford, R. D., & Begelman, M. C. 1999, *MNRAS*, 303, L1
- Blanton, E. L., Sarazin, C. L., & Irwin, J. A. 2001, *ApJ*, 552, 106
- Böker, T. 2000, in “Massive Stellar Clusters”, eds. A. Lançon & C. Boily, (San Francisco: ASP), 227
- Bower, G. A., Wilson, A. S., Heckman, T. M., & Richstone, D. O. 1996, *AJ*, 111, 1901
- Broos, P., et al. 2000, User’s Guide for the **TARA** Package: Document Revision 5.8 (University Park: Penn State University), <http://www.astro.psu.edu/xray/docs>
- Carollo, M. 1999, *ApJ*, 523, 566
- Cerviño, M., Mas-Hesse, J. M., & Kunth, D. 1997, *RMxAA* (Conf. Ser.), 6, 188
- Chu, Y.-H., & Mac Low, M.-M. 1990, *ApJ*, 365, 510
- Chartas, G. et al. 2000, *ApJ*, 542, 655
- Cui, W., Feldkhun, D., & Braun, R. 1997, *ApJ*, 477, 693
- Dalton, W. W. & Sarazin, C. L. 1995, *ApJ*, 440, 280
- de Vaucouleurs, G., de Vaucouleurs, A., Corwin, H. G., Jr., Buta, R. J., Paturel, G., & Fouqué, R. 1991, *Third Reference Catalogue of Bright Galaxies* (New York: Springer)
- Dopita, M. A. & Sutherland, R. S. 1995, *ApJ*, 455, 468
- Dopita, M. A. et al. in “The Physics of LINERs in View of Recent Observations”, eds. M. Eracleous et al. (San Francisco: ASP), 44
- Dressler, A. 1987, *ApJ*, 317, 1
- Eracleous, M. & Halpern, J. P. 1994, *ApJS*, 90, 1
- Eracleous, M. & Halpern, J. P. 2001, *ApJ*, 554, 240
- Eracleous, M., Livio, M., & Binette, L. 1995, *ApJ*, 445, L1
- Eracleous, M., Patterson, J., & Halpern, J. P. 1991, *ApJ*, 370, 330
- Eracleous, M., Sambruna, R. M., & Mushotzky, R. F. *ApJ*, 537, 654
- Fabbiano, G., Zezas, A., & Murray, S. S. 2001, *ApJ*, in press (astro-ph/0102256)
- Faber, S. M., Wegner, G., Burstein, D., Davies, R. L., Dressler, A., Lynden-Bell, D., & Terlevich, R. J. 1989, *ApJS*, 69, 763
- Falcke, H., Nagar, N. M., Wilson, A. S., & Ulvestad, J. S. 2000, *ApJ*, 542, 197
- Ferland, G. J. & Netzer, H. 1983, *ApJ*, 264, 105
- Ferrarese, L., Pogge, R. W., Peterson, B. M., Merrit, D., Wandel, A., & Joseph, C. L. 2001, *ApJ*, submitted (astro-ph/0104380)
- Filippenko, A. V. 1996, in “The Physics of LINERs in View of Recent Observations”, eds. M. Eracleous et al. (San Francisco: ASP), 17
- Filippenko, A. V. & Terlevich, R. 1992, *ApJ*, 397, L79
- Freeman, P. E., Kashyap, V., Rosner, R., & Lamb, D. Q. 2001, *ApJ*, submitted
- Gebhardt, K. et al. 2000, *ApJ*, 539, L3
- Griffiths, R. E., Ptak, A. F., Feigelson, E. D., Garmire, G., Townsley, L., Brandt, W. N., Sambruna, R. M., & Bregman, J. N. 2000, *Science*, 290, 1325
- Halderson, E. L., Moran, E. C., Filippenko, A. V., & Ho, L. C. 2001, *AJ*, in press (astro-ph/0105069)
- Halpern, J. P. & Steiner, J. E. 1983, *ApJ*, 269, L37
- Heckman, T. M. 1980, *A&A*, 87, 152
- Helfand, D. J. & Moran, E. C. 2001, *ApJ*, 554, 27
- Hempellmann, A., Schmidt, J. H. M. M., Schultz, M., Rüdiger, G., & Stepien, K. 1995, *A&A*, 294, 515
- Ho, L. C. 1999, *ApJ*, 516, 672
- Ho, L. C. et al. 2001, *ApJ*, 549, L51
- Ho, L. C., Filippenko, A. V., & Sargent, W. L. W. 1997a, *ApJS*, 112, 315
- Ho, L. C., Filippenko, A. V., Sargent, W. L. W., & Peng, C. 1997b, *ApJS*, 112, 391

- Ho, L. C., Filippenko, A. V., & Sargent, W. L. W. 1997c, *ApJ*, 487, 568
- Ho, L., Rudnick, G., Rix, H.-W., Shields, J. C., McIntosh, D. H., Filippenko, A. V., Sargent, W. L. W., & Eracleous, M. 2000, *ApJ*, 000, 000
- Hornschemeier, A. E. et al. 2001, *ApJ*, in press (astro-ph/0101494)
- Kastra, J. S. 1992, An X-Ray Spectral Code for Optically Thin Plasmas (Internal SRON-Leiden Report, updated version 2.0)
- King, A. R., Davies, M. B., Ward, M. J., Fabbiano, G., & Elvis, M. 2001, *ApJ*, 552, L109
- Komossa, S., Böhringer, H., & Huchra, J. P. 1999, *A&A*, 349, 88
- Lasota, J. P., et al 1996, *ApJ*, 462, 142
- Liedahl, D. A., Osterheld, A. I., & Goldstein, W. H. 1995, *ApJ*, 438, 115
- Lira, P., Ward, M., Zezas, A., Alonso-Herrero, A. & Ueno, S. 2001, *MNRAS*, in press (astro-ph/0109198)
- Mc Elroy, D. B. 1995, *ApJS*, 100, 105
- Maoz, D., Filippenko, A. V., Ho, L. C., Rix, H.-W., Bahcall, J. N., Schneider, D. P., & Macchetto, D. 1995, *ApJ*, 440, 91
- Maoz, D., Filippenko, A. V., Ho, L. C., Macchetto, D., Rix, H.-W., & Schneider, D. P., 1996, *ApJS*, 107, 215
- Maoz, D., Koratkar, A., Shields, J. C., Ho, L. C., Filippenko, A. V., & Sternberg, A. 1998, *AJ*, 116, 55
- Merrit, D. & Ferrarese, L. 2001, *ApJ*, 547, 140
- Mewe, R., Gronenschild, E. H. B. M., & van den Oord, G. H. J. 1985, *A&AS*, 62, 197
- Mewe, R., Lemen, J. R., & van den Oord, G. H. J. 1986, *A&AS*, 65, 511
- Mitsuda, K. et al. 1984, *PASJ*, 36, 741
- Mitsuda, K. H., Inoue, H., Nakamura, N., & Tanaka, Y. 1989, *PASJ*, 41, 97
- Modet, D. et al. 1996, USNO-SA2.0, U.S. Naval Observatory, Washington, D.C.
- Morrison, R. & McCammon, D. 1983, *ApJ*, 270, 119
- Mushotzky, R., Angelini, L., Arnaud, K., & Lowenstein, M. 2000, *HEAD*, 32, 2102
- Nandra, K., George, I. M., Mushotzky, R. F., Turner, T. J., & Yaqoob, T. 1997, *ApJ*, 476, 70
- Nagase, F. 1989, *PASJ*, 41, 1
- Narayan, R. & Yi, I. 1994, *ApJ*, 428, L13
- Narayan, R. & Yi, I. 1995, *ApJ*, 444, 231
- Narayan, R., Yi, I., & Mahadevan, R. 1996, *A&AS*, 120, C287
- Pogge, R. W. 1989, *ApJS*, 71, 433
- Pogge, R. W., Maoz, D., Ho, L. C., & Eracleous, M. 2000, *ApJ*, 532, 323
- Primini, F. A., Forman, W., & Jones, C. 1993, *ApJ*, 410, 615
- Ptak, A., Yaqoob, T., Mushotzky, R., Serlemitsos, P., & Griffiths, R. 1998, *ApJ*, 501, L37
- Ptak, A., Serlemitsos, P. J., Mushotzky, R. F., & Yaqoob, T. 1999, *ApJS* 120, 179
- Roberts, T. P., Warwick, R. S., & Ohashi, T. 1999, *MNRAS*, 304, 52
- Roberts, T. P., Schurch, N. J., & Warwick, R. S., 2001, *MNRAS*, 324, 737
- Sarazin, C. L., Irwin, J. A., & Bregman, J. N. 2001, *ApJ*, in press (astro-ph/0104070)
- Schlegel, D. J., Finkbeiner, D. P., Davis, M. 1998, *ApJ*, 500, 525
- Shields, J. C. 1992, *ApJ*, 399, L27
- Shields, J. C., Rix, H.-W., McIntosh, D. H., Ho, L. C., Rudnick, G., Filippenko, A. V., Sargent, W. L. W., & Sarzi, M. 2000, *ApJ*, 534, L27
- Sipior, M., & Eracleous, M. 2000, *HEAD*, 32, 1507
- Smith, B. J., Harvey, P. M., Colomé, C., Zhang, C. Y., DiFrancesco, J., & Pogge, R. W. 1994, *ApJ*, 425, 91
- Stark, A. A., Gammie, C. F., Wilson, R. W., Bally, J., Linke, R. A., Heiles, C., & Hurwitz, M. 1992, *ApJS*, 79, 77
- Taniguchi, Y., Ohya, Y., Yamada, T., Mouri, H., & Yoshida, M. 1996, *ApJ*, 467, 215
- Tennant, A. F., Wu, K., Ghosh, K. K., Kolodziejczak, J. J., & Schwartz, D. A. 2001, *ApJ*, 549, L43
- Terashima, Y., Kunieda, H., Misaki, K., Mushotzky, R. F., Ptak, A. F., & Reichert, G. A. 1998, *ApJ*, 503, 212
- Terashima, Y., Ho, L. C., Ptak, A. F., Mushotzky, R. F., Serlemitsos, P. J., & Yaqoob, T. 2000b, *ApJ*, 533, 729
- Terashima, Y., Ho, L. C., Ptak, A. F., Yaqoob, T., Kunieda, H., Misaki, K., & Serlemitsos, P. J. 2000c, *ApJ*, 535, L79
- Terlevich, R. & Melnick, J. 1985, *MNRAS*, 213, 841
- Titarchuk, L. 1994, *ApJ*, 434, 450
- Tozzi, P. et al. 2001, *ApJ*, submitted (astro-ph/0103198)
- Tully, R. B. 1998, *Nearby Galaxies Catalog* (Cambridge: Cambridge Univ. Press)
- Turner, J. L. & Ho, P. T. P. 1994, *ApJ*, 421, 122
- Van Bever, J. & Vanbeveren, D. 2000, *A&A*, 358, 462
- Wang, Q., Hamilton, T., Helfand, D. J., & Wu, X. 1991, *ApJ*, 374, 475
- Wang, Q. & Helfand, D. J. 1991, *ApJ*, 370, 541
- Ward, M. J., Zezas, A., Lira, P., Prestwich, A., Murray, S., Alonso-Herrero, A., & Ueno, S. 2000, *HEAD*, 32, 1805
- White, N. E., Stella, L., & Parmar, A. N. 1988, *ApJ*, 324, 363
- Storchi-Bergmann, T., Baldwin, J. A., & Wilson, A. S. 1993, *ApJ*, 410, L11
- Woo, J. W., Clark, G. W., & Levine, A. 1995, *ApJ*, 449, 880

TABLE 1
TARGETS AND THEIR BASIC PROPERTIES

Target Name(s)	Hubble Type ^a	Distance ^b (Mpc)	Spatial Scale (pc/'')	Galactic N_{H} ^c (10^{20} cm^{-2})	Galactic $E(B - V)$ ^d (mag)	v_{\odot} ^e (km s^{-1})
NGC 404	SA(s)0-	2.4	12	5.30	0.059	-46
NGC 4736 (M94)	(R)SA(r)ab	4.3	21	1.41	0.018	307
NGC 4579 (M58)	SAB(rs)b	16.8	81	2.54	0.041	1521

References. — (a) de Vaucouleurs et al. (1991), (b) Tully (1988), (c) Stark et al. (1992), (d) Schlegel, Finkbeiner, & Davis (1998), (e) Ho et al. (1997a)

TABLE 2
OBSERVATION LOG

Target	Observation Start (UT)	Exposure Time (s)
NGC 404	1999 Dec 19, 21:12:43	23,864
NGC 4736	2000 May 13, 03:12:11	47,366
NGC 4579	2000 May 02, 16:26:44	33,905

TABLE 3
PARAMETERS OF THERMAL PLASMA MODELS

Model Parameters	NGC 404 ^a	NGC 4736 ^b	NGC 4579 ^b	
			$Z = \text{free}$	$Z = Z_{\odot}$
N_{H} (10^{20} cm^{-2})	< 6	1.4 ^c	< 6	7_{-4}^{+9}
Abundance (Z/Z_{\odot})	< 0.12	$0.3_{-0.2}^{+1.4}$	$0.2_{-0.1}^{+1.3}$	1 (fixed)
kT ^d (keV)	$0.6_{-0.4}^{+0.3}$	0.56 ± 0.06	0.3 ± 0.2 , $0.6_{-0.1}^{+0.4}$, > 6	$0.11_{-0.04}^{+0.05}$, $0.58_{-0.08}^{+0.04}$, 10_{-4}^{+44}
EM ^e (10^{61} cm^{-3})	0.35	0.7	33, 34, 28	34, 11, 27
Total χ^2	10.45	3.159	22.507	25.546
Reduced χ^2	0.696	0.632	1.072	1.161
Flux ($\text{erg cm}^{-2} \text{ s}^{-1}$)				
0.5-2 keV	1.5×10^{-14}	2.0×10^{-14}	1.2×10^{-13}	
2-10 keV	1.2×10^{-13}	
Luminosity (erg s^{-1})				
0.5-2 keV	1.0×10^{37}	4.4×10^{37}	4.1×10^{39}	
2-10 keV	4.1×10^{39}	

^a The spectrum was extracted from a circular region of area 13 square arcseconds, equal to the area of a point source.

^b The spectrum was extracted from a region of area 239 square arcseconds.

^c Held fixed at the Galactic value because it was unconstrained.

^d Single-temperature models for NGC 404 and NGC 4736, 3-temperature model for NGC 4579.

^e Emission measure: $EM = \int n_e n_i dV$, where n_e and n_i are the electron and ion densities.

TABLE 4
POWER-LAW FITS TO SPECTRA OF BRIGHT DISCRETE SOURCES

Object	Column Density (10^{20} cm^{-2})	Power-Law Photon Index	Observed 2–10 keV Flux ($\text{erg cm}^{-2} \text{ s}^{-1}$)	2–10 keV Luminosity ^a (erg s^{-1})	Total χ^2	Reduced χ^2
<i>NGC 4736</i>						
X-1	< 3.7	1.13 ± 0.10	6.4×10^{-13}	1.4×10^{39}	34.13	0.7937
X-2	< 3.3	1.6 ± 0.1	2.7×10^{-13}	5.9×10^{38}	20.92	0.9511
X-3	10^{+13}_{-9}	$1.8^{+0.7}_{-0.4}$	2.3×10^{-13}	5.1×10^{38}	30.19	1.078
X-4	< 12	1.6 ± 0.2	1.4×10^{-13}	3.1×10^{38}	23.08	0.9234
<i>NGC 4579</i>						
X-1	18^{+6}_{-4}	1.8 ± 0.2	2.7×10^{-13}	9.1×10^{39}	22.05	0.9588

^a Intrinsic luminosity, corrected for absorption.

TABLE 5
VARIABILITY PROPERTIES OF BRIGHT X-RAY SOURCES

Object	Excess Variance (s^{-1})	Maximum Pulsed Fraction (%)
<i>NGC 4736</i>		
X-1	0.06 ± 0.02	13
X-2	0.06 ± 0.04	10
X-3	0.10 ± 0.07	17
X-4	< 0.1	19
<i>NGC 4579</i>		
AGN (0.5–1 keV)	0.035 ± 0.008	...
AGN (0.5–8 keV)	0.017 ± 0.001	...
AGN (0.5–8 keV), PSF wings	0.05 ± 0.02	...
X-1 (UXB)	< 0.02	18

TABLE 6
CATALOG OF DISCRETE SOURCES IN NGC 4736

Official Name (CXOU J)	Alias	Coordinates (J2000)	Count Rate (10^{-2} s^{-1})	Color	$L_X(0.5\text{--}8 \text{ keV})$ ($10^{37} \text{ erg s}^{-1}$)
125041.7 + 410556		12:50:41.8 +41:05:56	0.035 ± 0.009	0.6 ± 0.2	0.29
125047.6 + 410512		12:50:47.6 +41:05:12	0.35 ± 0.03	0.34 ± 0.04	3.50
125047.7 + 410707		12:50:47.7 +41:07:08	0.05 ± 0.01	< 0.4	0.52
125048.6 + 410742		12:50:48.6 +41:07:42	0.51 ± 0.03	0.11 ± 0.01	6.00
125048.8 + 410635		12:50:48.8 +41:06:36	0.010 ± 0.006	< 1.2	0.07
125049.9 + 410640		12:50:50.0 +41:06:41	0.09 ± 0.02	< 0.3	0.93
125050.2 + 410752		12:50:50.3 +41:07:53	0.06 ± 0.01	< 0.4	0.64
125050.3 + 410712	X-4	12:50:50.3 +41:07:12	2.67 ± 0.08	0.34 ± 0.01	31.00
125050.3 + 410628		12:50:50.3 +41:06:28	0.05 ± 0.01	< 0.4	0.49
125050.7 + 410738		12:50:50.8 +41:07:38	0.20 ± 0.02	< 0.2	2.20
125051.0 + 410742		12:50:51.0 +41:07:43	0.05 ± 0.01	< 0.5	0.44
125051.0 + 410646		12:50:51.1 +41:06:47	0.19 ± 0.02	< 0.2	2.20
125052.0 + 410716		12:50:52.1 +41:07:16	0.03 ± 0.01	< 1.3	0.20
125052.0 + 410654		12:50:52.1 +41:06:55	0.24 ± 0.03	0.47 ± 0.08	2.20
125052.5 + 410714		12:50:52.6 +41:07:15	0.84 ± 0.05	0.50 ± 0.05	7.40
125052.5 + 410701		12:50:52.6 +41:07:02	1.49 ± 0.06	< 0.06	17.00
125052.7 + 410718	X-3	12:50:52.7 +41:07:19	4.6 ± 0.1	0.272 ± 0.009	51.00
125052.9 + 410745		12:50:52.9 +41:07:46	0.08 ± 0.02	< 0.3	0.78
125052.9 + 410707		12:50:53.0 +41:07:07	0.12 ± 0.03	< 0.4	1.10
125053.0 + 410712	X-2	12:50:53.1 +41:07:13	5.4 ± 0.1	0.176 ± 0.008	59.00
125053.2 + 410718		12:50:53.3 +41:07:18	0.06 ± 0.02	< 0.7	0.41
125053.2 + 410659		12:50:53.3 +41:06:60	0.32 ± 0.03	0.19 ± 0.03	3.60
125053.3 + 410713	X-1	12:50:53.3 +41:07:14	9.4 ± 0.1	0.44 ± 0.01	140.00
125053.3 + 410702		12:50:53.3 +41:07:03	0.11 ± 0.02	0.35 ± 0.10	1.10
125053.7 + 410718		12:50:53.7 +41:07:19	1.39 ± 0.06	0.37 ± 0.02	14.00
125053.7 + 410713		12:50:53.8 +41:07:13	0.28 ± 0.03	0.22 ± 0.04	3.00
125054.0 + 410629		12:50:54.1 +41:06:30	0.19 ± 0.02	< 0.2	2.20
125054.3 + 410746		12:50:54.4 +41:07:47	0.33 ± 0.03	0.59 ± 0.08	2.70
125054.5 + 410636		12:50:54.6 +41:06:37	0.03 ± 0.01	< 0.6	0.26
125055.0 + 410634		12:50:55.0 +41:06:34	0.05 ± 0.01	< 0.5	0.47
125055.2 + 410831		12:50:55.2 +41:08:31	0.04 ± 0.01	< 0.4	0.42
125055.6 + 410719		12:50:55.6 +41:07:20	0.28 ± 0.03	< 0.1	3.20
125055.7 + 410704		12:50:55.7 +41:07:05	0.04 ± 0.01	< 0.5	0.34
125056.3 + 410655		12:50:56.3 +41:06:55	1.05 ± 0.05	0.60 ± 0.04	8.50
125056.8 + 410705		12:50:56.8 +41:07:06	0.016 ± 0.007	< 1.0	0.10
125058.4 + 410813		12:50:58.4 +41:08:14	0.014 ± 0.006	< 1.2	0.09
125101.9 + 410855		12:51:02.0 +41:08:56	0.025 ± 0.008	< 0.7	0.19
125104.0 + 410738		12:51:04.1 +41:07:39	0.041 ± 0.009	< 0.5	0.34
125111.0 + 410850		12:51:11.1 +41:08:50	0.06 ± 0.01	0.4 ± 0.1	0.54

TABLE 7
CATALOG OF DISCRETE SOURCES IN NGC 4579

Official Name (CXOU J)	Alias	Coordinates (J2000)	Count Rate (10^{-2} s^{-1})	Color	$L_X(0.5-8 \text{ keV})$ ($10^{37} \text{ erg s}^{-1}$)
123739.7 + 114806		12:37:39.8 +11:48:06	0.016 ± 0.006	< 0.9	1.60
123740.2 + 114648		12:37:40.3 +11:46:48	0.027 ± 0.008	< 0.9	2.80
123740.2 + 114727	X-1	12:37:40.3 +11:47:27	3.30 ± 0.08	0.35 ± 0.01	1050.00
123740.4 + 114835		12:37:40.4 +11:48:36	0.034 ± 0.009	0.8 ± 0.3	3.80
123741.9 + 115004		12:37:41.9 +11:50:05	0.07 ± 0.01	< 0.4	10.00
123742.3 + 114909		12:37:42.3 +11:49:09	0.04 ± 0.01	< 0.6	4.60
123742.6 + 114825		12:37:42.6 +11:48:25	0.024 ± 0.008	< 0.9	2.40
123742.7 + 114945		12:37:42.8 +11:49:45	0.04 ± 0.01	0.7 ± 0.3	5.40
123743.0 + 114759		12:37:43.0 +11:47:60	0.020 ± 0.007	< 1.0	1.90
123743.2 + 114901		12:37:43.2 +11:49:01	0.42 ± 0.04	0.27 ± 0.04	70.00
123743.2 + 114912		12:37:43.2 +11:49:13	0.05 ± 0.01	< 0.7	6.00
123743.7 + 114824		12:37:43.7 +11:48:25	0.09 ± 0.01	0.34 ± 0.09	14.00
123744.1 + 114917		12:37:44.1 +11:49:17	0.11 ± 0.02	0.5 ± 0.1	15.00
123744.3 + 114834		12:37:44.3 +11:48:35	0.032 ± 0.009	< 0.7	3.90
123744.5 + 114921		12:37:44.5 +11:49:22	0.08 ± 0.02	1.0 ± 0.3	8.00
123745.3 + 114818		12:37:45.4 +11:48:19	0.025 ± 0.008	< 0.9	2.50
123746.3 + 114958		12:37:46.3 +11:49:59	0.04 ± 0.01	0.7 ± 0.3	5.30
123746.4 + 115012		12:37:46.5 +11:50:13	0.011 ± 0.005	< 1.1	1.10
123746.8 + 114831		12:37:46.8 +11:48:32	0.027 ± 0.008	< 0.9	2.80
123747.4 + 115105		12:37:47.5 +11:51:06	0.07 ± 0.01	0.4 ± 0.1	10.00
123753.8 + 115020		12:37:53.9 +11:50:20	0.29 ± 0.03	0.24 ± 0.03	50.00

TABLE 8
POWER BUDGET

	0.5–10 keV Luminosity (erg s^{-1})		
	NGC 404	NGC 4736	NGC 4579
AGN	2.9×10^{41}
Diffuse or Thermal Emission ^a	1×10^{37}	6×10^{38}	1.6×10^{40}
UXBs	1.3×10^{40}
Other discrete sources	...	3.7×10^{39}	2×10^{39}
<i>Chandra</i> Total	1×10^{37}	4×10^{39}	3.2×10^{41}
<i>ASCA</i> Total ^b	$< 5 \times 10^{37}$	3×10^{39}	3.0×10^{41}

^a This is the *total* luminosity of the entire diffuse source, estimated after subtracting the contribution of point sources embedded in it.

^b References. – NGC 404: Roberts et al. (2001); NGC 4736: Roberts et al. (1999); NGC 4579: Terashima et al. (1998)

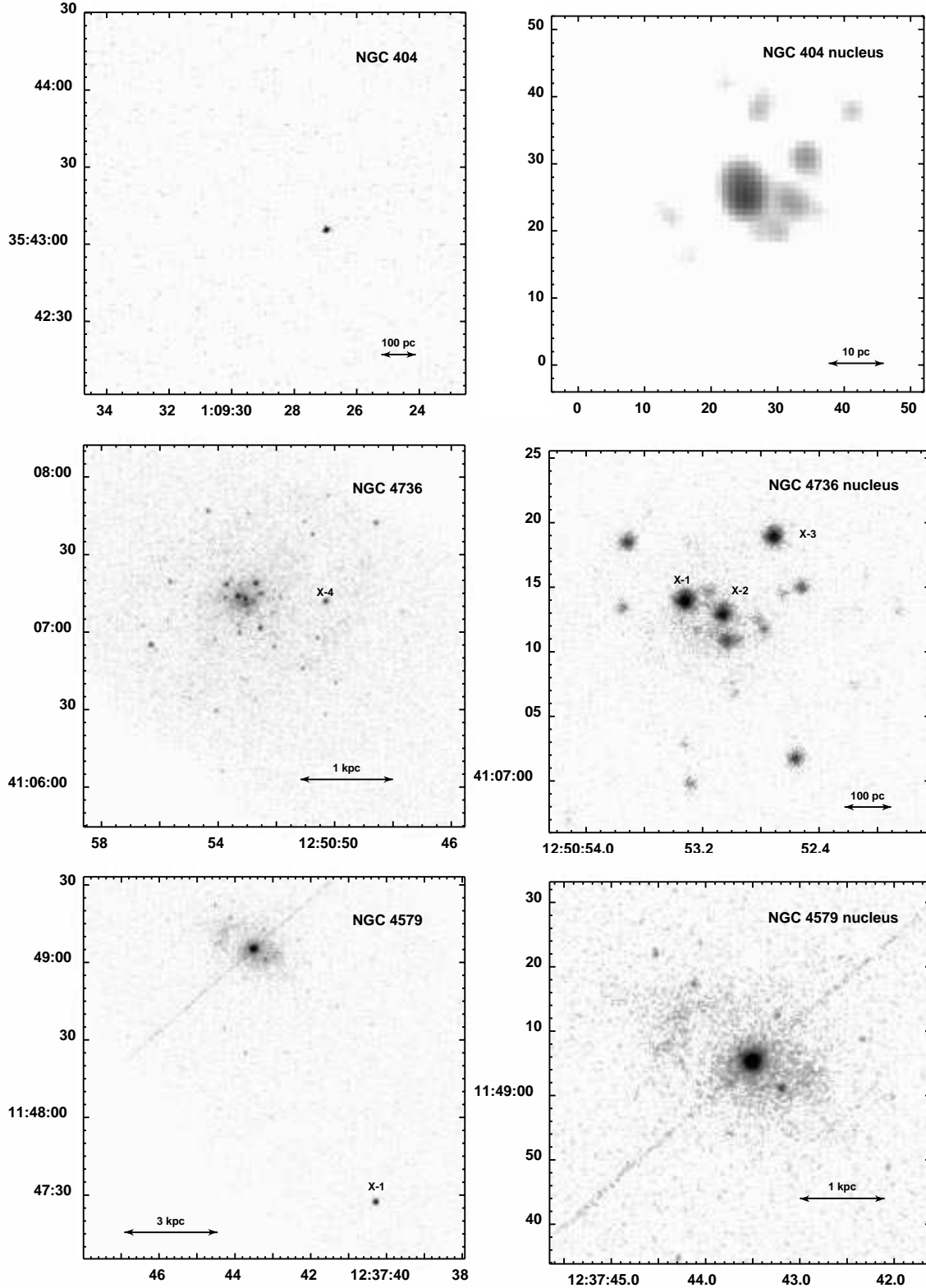


FIG. 2.— Montage of *Chandra* images of the target galaxies. For each galaxy we show an image encompassing all the interesting features in the field of view as well as an enlarged view of the nucleus. All but one of the frames are labeled with the right ascension along the horizontal axis and the declination along the vertical axis (the coordinate epoch is J2000, north is up, and east is to the left). The image of the nucleus of NGC 404 has been deconvolved using the Lucy-Richardson algorithm; its frame is calibrated in pixels, where each pixel corresponds to $0''.15$. The discrete “blobs” around the nucleus of NGC 404 are not discernible in the original, unprocessed image. A horizontal bar in each image gives the linear scale at the distance of that galaxy. Bright X-ray sources, referred to in the text and in the tables, are labeled on the images.

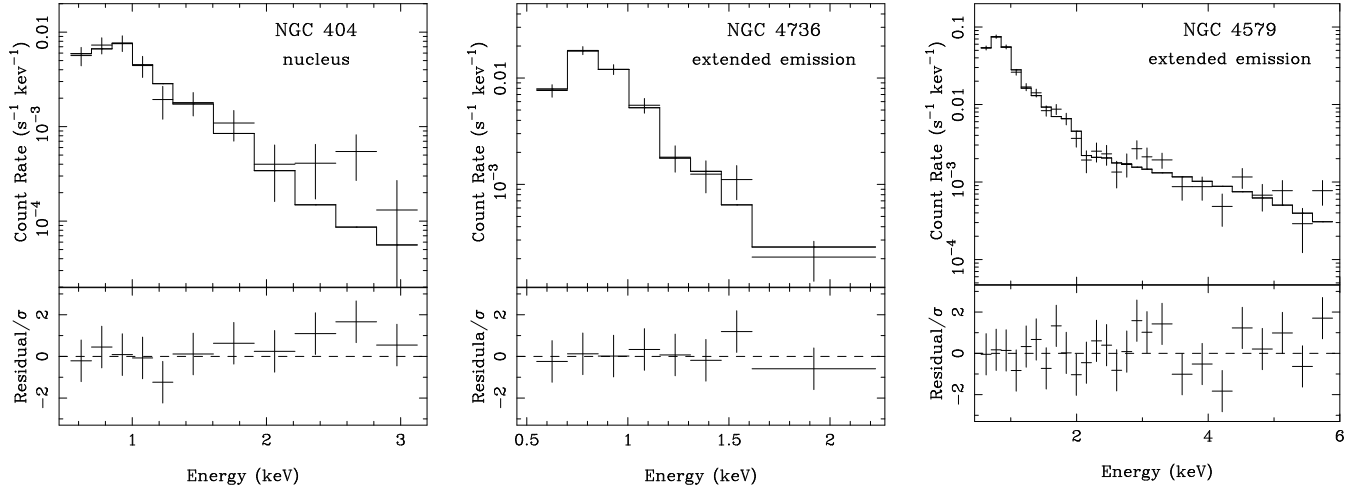


FIG. 3.— Spectra of the thermal plasma regions in the three target galaxies, the nucleus of NGC 404 and the extended, circumnuclear emission in NGC 4736 and NGC 4579. For each object we show the observed spectrum with the best-fitting model superposed (upper panel) and the post-fit residuals scaled by the error bar (lower panel). The models consist of linear combinations of thermal plasma components, with abundances left as free parameters (1 component in NGC 404 and NGC 4736, and 3 components in NGC 4579). The parameters describing these models are summarized in Table 3.

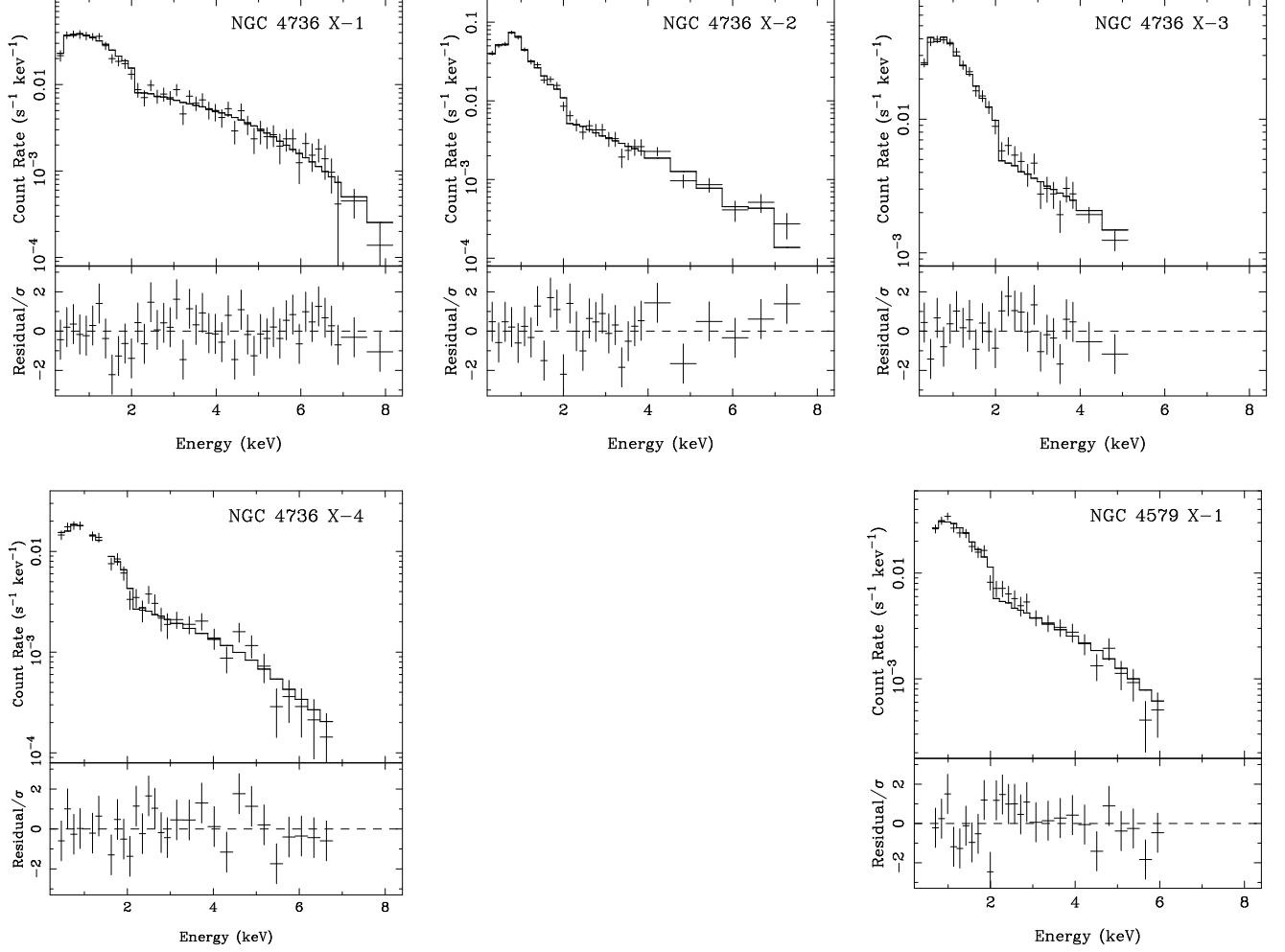


FIG. 4.— Spectra of the brightest X-ray binaries in NGC 4736 and NGC 4579. The objects are labeled according to the conventions defined in Tables 6 and 7. For each object we show the observed spectrum with the best-fitting model superposed (upper panel) and the post-fit residuals scaled by the error bar (lower panel). The parameters describing the best-fitting models are summarized in Table 4.

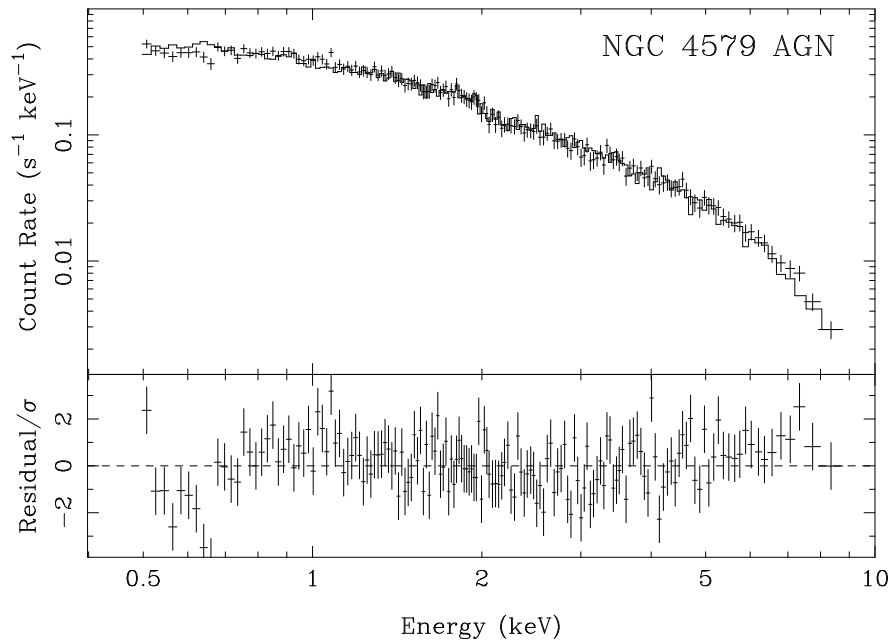


FIG. 5.— Spectrum of the AGN in NGC 4579 with the best-fitting model superposed. The model consists of a simple power law modified by photoelectric absorption in the Galaxy, as described in §5.4. The lower panel shows the residuals scaled by the error bar at each bin. The large residuals around 0.6 keV may be the result of poor calibration of the S3 CCD. Due to calibration uncertainties, we are not able to assess the reality of this feature.

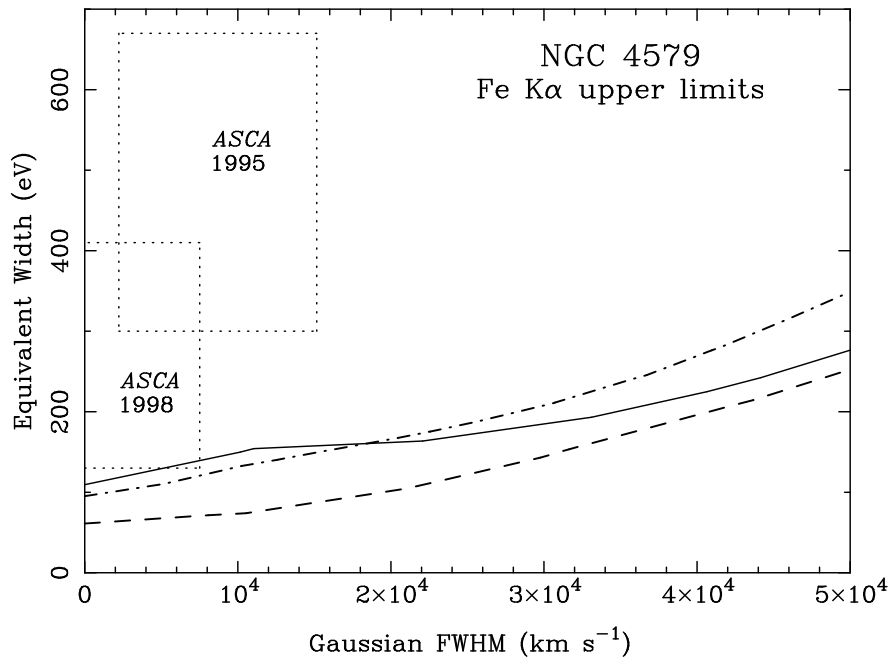


FIG. 6.— Confidence contours showing the 99% upper limits on the equivalent width of the Fe $K\alpha$ line in the spectrum of the AGN in NGC 4579 as a function of its FWHM. The equivalent width scale has been corrected for the effect of pileup by multiplying all values by $1 + f_p$, where f_p is the pileup fraction in the 6–7 keV band (see §5.4 of the test for a detailed discussion). The three curves refer to different assumed line energies; solid curve: 6.4 keV, dashed curve: 6.7 keV, dot-dashed curve: 6.9 keV. The error boxes (dotted lines corresponding to the 90% confidence regions) show the measurements from *ASCA* observations (Terashima et al. 1998, 2000c) with dates as marked.

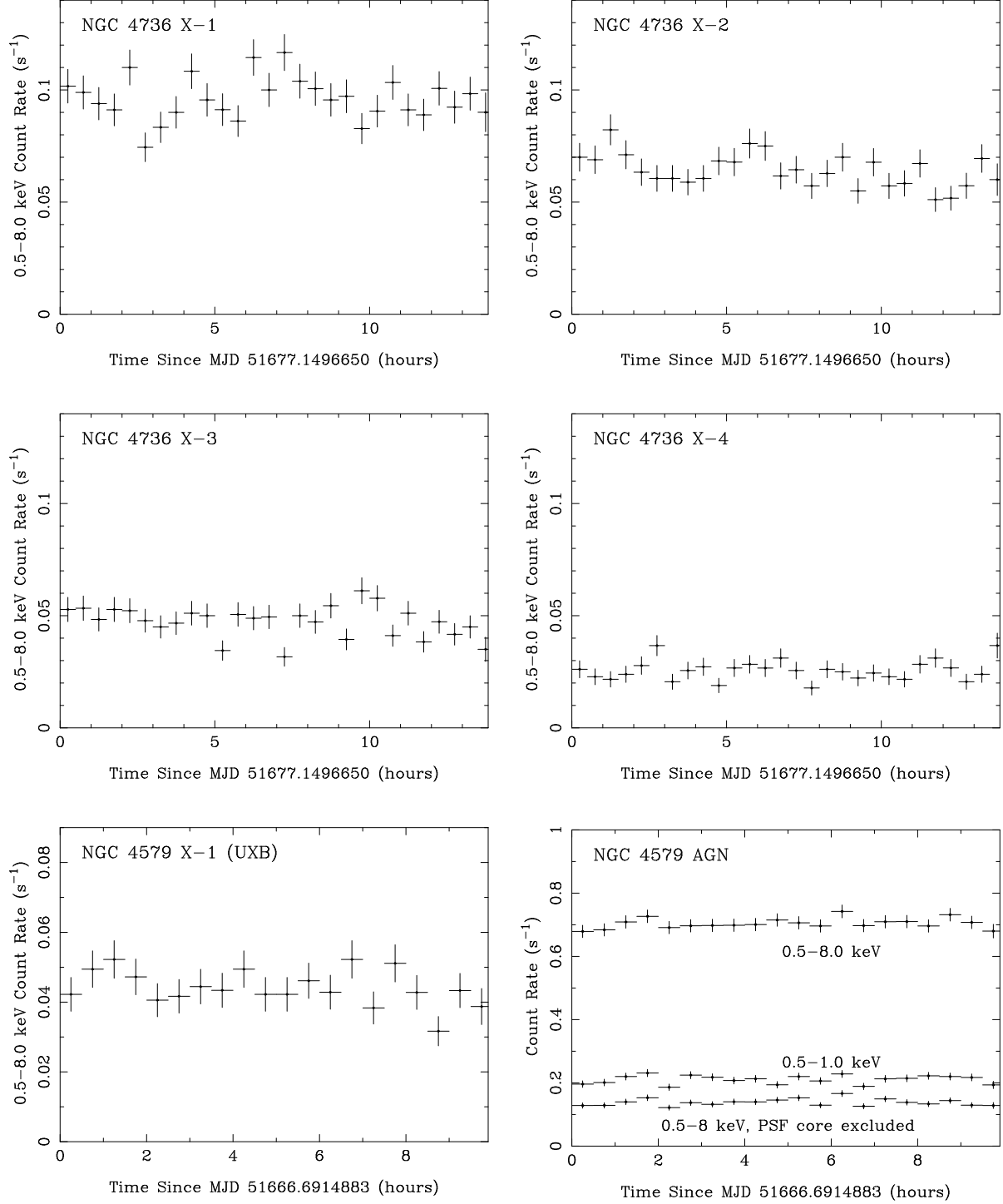


FIG. 7.— Light curves of bright point sources in NGC 4736 and NGC 4579. The objects are labeled according to the conventions defined in Tables 6 and 7. In the case of the AGN in NGC 4579, we plot the 0.5–1.0 keV and 0.5–8.0 keV light curves, as well as the 0.5–8.0 keV light curve extracted from the wings of the PSF. In all other cases we plot only the 0.5–8.0 keV light curves.

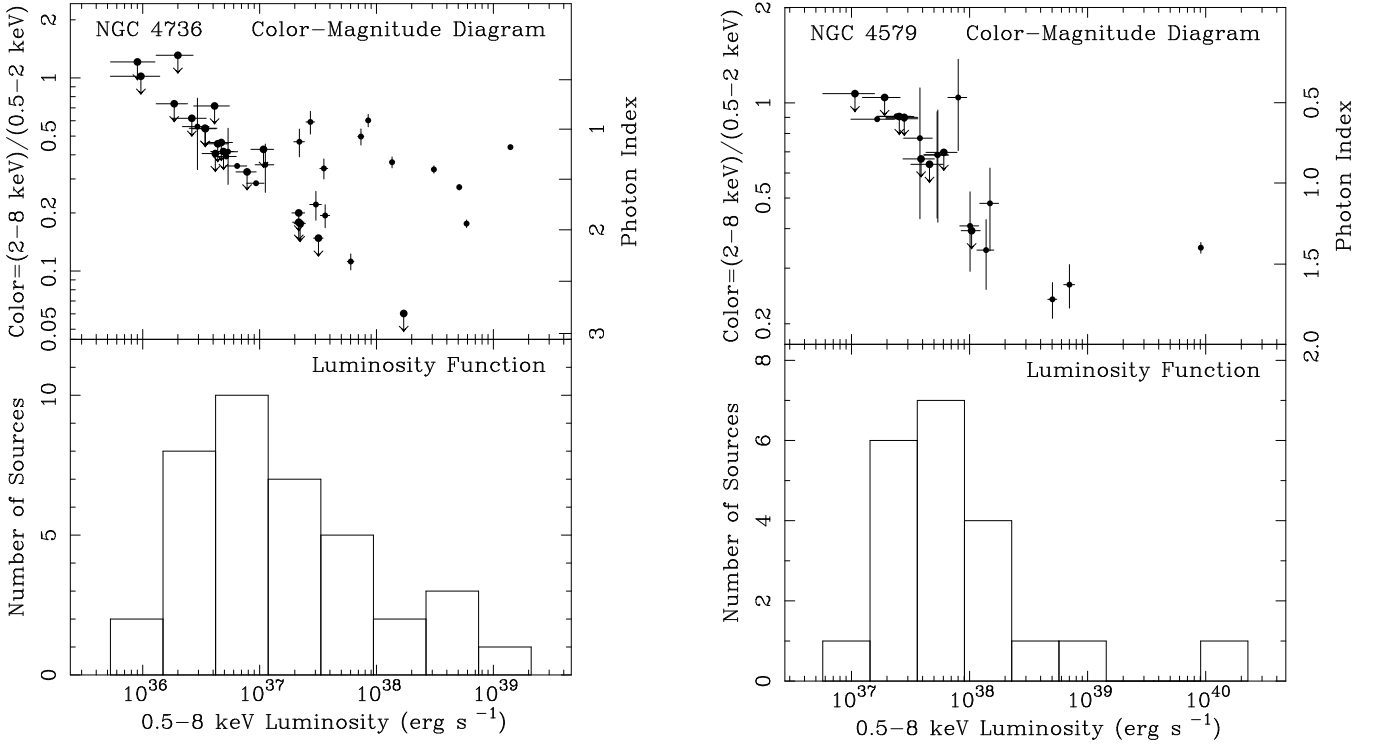


FIG. 8.— Color-Magnitude diagrams and luminosity distributions for the X-Ray binaries in NGC 4579 and NGC 4736. In the top frame of each set the vertical axis is calibrated in color (left) and in spectral index (right). Upper limits to the color are denoted by arrows.

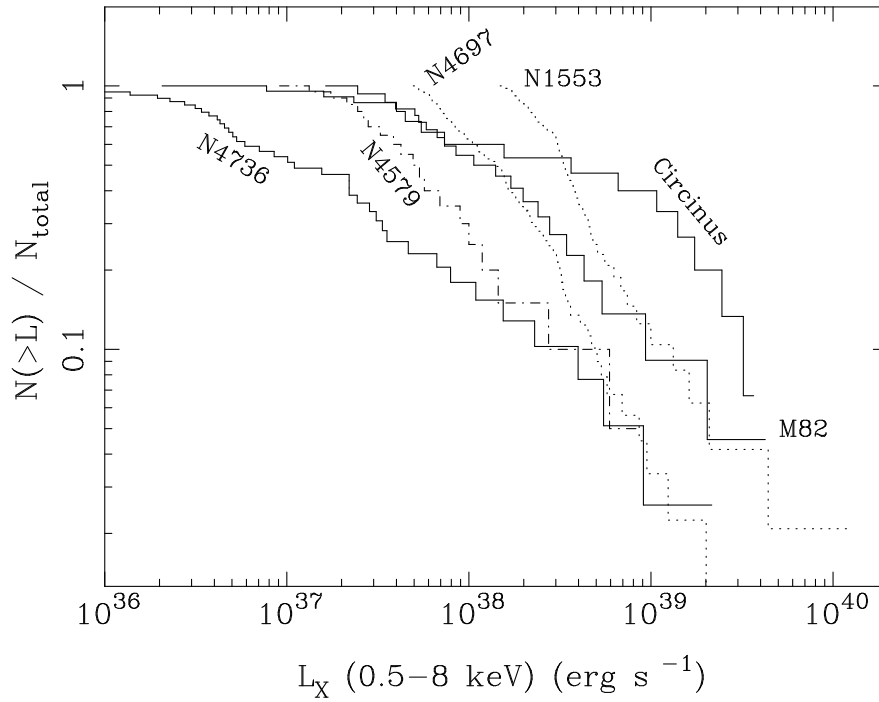


FIG. 9.— Cumulative X-ray source luminosity functions of NGC 4579 (dot-dashed line) and NGC 4736 (solid line) compared to those of other galaxies observed by *Chandra*. The comparison galaxies are NGC 4697 and NGC 1553 (E and S0, dotted lines), and M82 and Circinus (starbursting spirals, solid lines). The UXB in NGC 4579 is excluded from its luminosity function in the interest of clarity.